



## Volatile organic compounds (VOCs) in photochemically aged air from the Eastern and Western Mediterranean

Bettina Derstroff<sup>1</sup>, Imke Hüser<sup>1</sup>, Rolf Sander<sup>1</sup>, Efstratios Bourtsoukidis<sup>1</sup>, John N. Crowley<sup>1</sup>, Horst Fischer<sup>1</sup>, Sergey Gromov<sup>1</sup>, Hartwig Harder<sup>1</sup>, Jürgen Kesselmeier<sup>1</sup>, Jos Lelieveld<sup>1</sup>, Chinmay Mallik<sup>1</sup>, Monica Martinez<sup>1</sup>, Anna Novelli<sup>3</sup>, Uwe Parchatka<sup>1</sup>, Gavin J. Phillips<sup>2</sup>, Carina Sauvage<sup>1</sup>, Jan Schuladen<sup>1</sup>, Christof Stöner<sup>1</sup>, Laura Tomsche<sup>1</sup>, and Jonathan Williams<sup>1</sup>

<sup>1</sup>Max Planck Institute for Chemistry, Mainz, Germany

<sup>2</sup>University of Chester, United Kingdom

<sup>3</sup>Forschungszentrum Jülich, Germany

*Correspondence to:* Bettina Derstroff (bettina.derstroff@mpic.de), Jonathan Williams (jonathan.williams@mpic.de)

**Abstract.** During the summertime CYPHEX campaign (CYprus PHotochemical EXperiment 2014) in the Eastern Mediterranean, multiple volatile organic compounds (VOCs) were measured from a 650 m hilltop site in western Cyprus (34° 57' N/32° 23' E). Periodic shifts in the northerly Etesian winds resulted in the site being alternately impacted by photochemically processed emissions from Western (Spain, France, Italy) and Eastern (Turkey, Greece) Europe. In this study we examine the temporal variation of VOCs at the site. The sparse Mediterranean scrub vegetation generated diel cycles in the reactive biogenic hydrocarbon isoprene, from below detection limit at night to 100 pptv by day on average. In contrast, the oxygenated volatile organic compounds (OVOCs) methanol and acetone exhibited no diel cycle and were approximately an order of magnitude higher in mixing ratio (range: 1–8 ppbv) than the locally emitted isoprene (up to 320 pptv), total monoterpenes (up to 250 pptv) and aromatic compounds such as benzene and toluene (up to 100 pptv, spikes up to 400 pptv). Acetic acid was present at mixing ratios between 0.05 and 4 ppbv and followed a pronounced diel cycle in one specific period, which was related to local production and loss and local meteorological effects. During the rest of the campaign the impact of the free troposphere and long distance transport from source regions dominated over local processes and diel cycles were not observed. The Lagrangian model FLEXPART was used to determine transport patterns and photochemical processing times of air masses originating from Eastern and Western Europe. Eastern and Western European air masses showed distinct trace gas concentrations, with ca. 20 % higher ozone and ca. 30-50 % higher values for most of the OVOCs observed from the East. Using the FLEXPART calculated transport time, the contribution of photochemical processing, sea surface



contact and dilution was estimated. Methanol, acetone and acetic acid all decreased with residence  
time in the marine boundary layer (MBL) with loss rates of  $0.1 \pm 0.01$  ppbv/h,  $0.06 \pm 0.01$  ppbv/h,  
 $0.05 \pm 0.01$  ppbv/h from Eastern Europe and  $0.06 \pm 0.01$  ppbv/h,  $0.02 \pm 0.004$  ppbv/h and  $0.03 \pm$   
0.004 ppbv/h from Western Europe, respectively. The most soluble species, acetic acid, showed the  
25 lowest loss rates, indicating that solubility limited deposition to the ocean was not the only factor  
and that turbulent transport, plume dilution, microbial consumption within the surface of the ocean  
and especially entrainment from the free troposphere may also be important. Correlations between  
acetone, methanol and acetic acid were rather weak in western air masses ( $r^2=0.52-0.62$ ), but were  
stronger in air masses measured after the shorter transport time from the East ( $r^2=0.53-0.81$ ).

30

Keywords: volatile organic compounds, Mediterranean, long distance transport, marine boundary  
layer, methanol, acetone, acetic acid, isoprene, monoterpenes

## 1 Introduction

The island of Cyprus is situated on the southeastern edge of the European Union. During the summer  
35 months, the east-west pressure gradient between the quasi-permanent South Asian monsoon low, the  
Persian trough and the Azores high induces northerly winds (Etesians), that overcome the westerly  
flow that is typical at temperate latitudes. The varying influences from the westerly and northerly  
winds make Cyprus an ideal vantage point to examine photochemically processed air from Eastern  
and Western Europe. Despite a modest population (1.15 million<sup>1</sup>) and little industrial emissions,  
40 the EU ozone air quality standard is regularly exceeded (Kourtidis et al., 2002; Kouvarakis et al.,  
2002; Gerasopoulos et al., 2005; Kalabokas et al., 2007, 2008, 2013; Doche et al., 2014; Kleant-  
hous et al., 2014). The excess ozone is formed in sunlit conditions when volatile organic compounds  
(VOC), emitted from countries to the north and west of Cyprus, are oxidized in the gas phase by  
45 the atmosphere's primary oxidant, the OH radical in the presence of NO<sub>x</sub> (NO + NO<sub>2</sub>) (Atkin-  
son, 1990). In addition to ozone, numerous other secondary oxidants are formed including a suite  
of oxidized volatile organic compounds (OVOCs) such as alcohols (e.g. methanol), carbonyls (e.g.  
acetone), and organic acids (e.g. acetic acid). In this study we exploit the location and dual meteoro-  
logical flow regime to investigate the abundance, temporal behavior, dependence on origin and the  
50 marine influence on VOCs. Several extensive studies of VOCs have been conducted previously in the  
Mediterranean area which have highlighted the relevance of anthropogenic, biogenic and biomass  
burning sources for regional chemistry. Airborne measurements have shown that the Mediterranean  
atmosphere is a cross-road for global pollution, with boundary layer chemistry driven by emissions  
from the European mainland, whereas the mid-troposphere (4–8 km) is influenced by North Amer-  
ican emissions and above this, monsoon outflow from Asia (Lelieveld et al., 2002). Measurements

<sup>1</sup><http://data.worldbank.org/country/cyprus>; accessed on 4 May 2016



55 made on Crete approximately one day downwind of mainland Greece revealed the enormous com-  
plexity of VOCs in the region (Xu et al., 2003). Moreover, it has been shown that the mixing ratios  
of many VOCs, especially OVOCs, in the Mediterranean strongly depend on long distance transport  
and are periodically influenced by biomass burning (Salisbury et al., 2003; Holzinger et al., 2005).  
Reactive biogenic species such as isoprene have also been shown to be emitted from Mediterranean  
60 vegetation (Kesselmeier et al., 1996; Liakakou et al., 2007).

Here we examine the relative impacts of biogenic emissions and long distance pollutant transport  
from Eastern and Western Europe on trace gas levels, with particular emphasis on VOCs. Moreover,  
we exploit the island location to investigate the influence of the sea on VOCs since air from East-  
ern and Western Europe was advected with variable transport times to the site within the marine  
65 boundary layer. The effect of the ocean on many VOCs, particularly OVOCs, can be significant and  
variable in latitude (Yang et al., 2013, 2014), biological activity (Taddei et al., 2009) and time of  
the day (Sinha et al., 2007). To this end we have examined the behavior of an alcohol (methanol), a  
carbonyl (acetone), and an acid (acetic acid).

Methanol is primarily emitted from plants (Galbally and Kirstine, 2002), with a relatively small pho-  
70 tochemical production term in the estimated global budget, 37 Tg yr<sup>-1</sup> from a total of 242 Tg yr<sup>-1</sup>  
(Millet et al., 2008). One of the main sinks of methanol is the oxidation by OH, while the role of the  
ocean is not completely characterized: Millet et al. (2008) report a methanol sink via OH oxidation  
of 88 Tg yr<sup>-1</sup> and an ocean uptake of 101 Tg yr<sup>-1</sup> of a total sink of 242 Tg yr<sup>-1</sup>. In contrast, Jacob et  
al. (2005) found a loss of methanol via the reaction with OH of 129 Tg yr<sup>-1</sup> while the ocean uptake  
75 amounts only to 10 Tg yr<sup>-1</sup> from a total sink of 206 Tg yr<sup>-1</sup>.

According to Fischer et al. (2012) the global acetone budget sums up to 146 Tg yr<sup>-1</sup>, 32 Tg yr<sup>-1</sup>  
being terrestrial emissions from biosphere and 31 Tg yr<sup>-1</sup> being photochemical production (26 Tg  
yr<sup>-1</sup> anthropogenic, 5 Tg yr<sup>-1</sup> biogenic). The main acetone sinks are photolysis and reaction with  
OH: Fischer et al. (2012) report a loss of 33 Tg yr<sup>-1</sup> by OH oxidation and 19 Tg yr<sup>-1</sup> by photolysis  
80 from a total sink of 146 Tg yr<sup>-1</sup>. Depending on the season and geographical location the ocean can  
either be a sink (82 Tg yr<sup>-1</sup>) or a source (80 Tg yr<sup>-1</sup>) of acetone and is globally in a near equilibrium  
state. Jacob et al. (2002) on the other hand determined a sink by OH reaction of 27 Tg yr<sup>-1</sup> and by  
photolysis of 46 Tg yr<sup>-1</sup> from a total loss of 95 Tg yr<sup>-1</sup>.

Most of the acetic acid budget is in-situ photochemical production, about 59 Tg yr<sup>-1</sup> from a total  
85 source of 86 Tg yr<sup>-1</sup>. The total acetic acid sink of 86 Tg yr<sup>-1</sup> consists of approximately 1/3 pho-  
tochemical loss (25 Tg yr<sup>-1</sup>), 1/3 wet deposition (27 Tg yr<sup>-1</sup>) and 1/3 dry deposition (31 Tg yr<sup>-1</sup>)  
(Paulot et al., 2011).

Using the rate coefficient (k) for each OVOC provided by IUPAC (Atkinson et al., 2006) and the  
diel mean OH concentration of  $2 \times 10^6$  molec cm<sup>-3</sup> measured during the campaign, the following  
90 atmospheric lifetimes with respect to the removal by OH were calculated: 6 days for methanol, 32  
days for acetone and 8 days for acetic acid.



The novelty of the CYPHEX (CYprus PHotochemical EXperiment) campaign for VOC research was threefold: firstly, Eastern and Western European outflow was chemically characterized and contrasted; secondly, the relative local impacts on biogenic and transported VOCs were assessed and  
95 thirdly, the influence of summertime Mediterranean marine boundary layer transport on OVOCs was investigated.

## 2 Experimental

### 2.1 Site

The measurement site (Ineia) is situated on the northwest coast of Cyprus at the top of a 650 m hill  
100 located ca. 10 km from the shoreline (34°57' N/32°23' E). The surrounding area (5 km radius) is rural in character, comprising of farmland and a few small villages (e.g Ineia population 367<sup>2</sup>). Extending 25 km to the northwest was the Akamas peninsula national park and to the northeast the terrain descended rapidly to the city of Polis (population 1975<sup>2</sup>) at sea level. The vegetation is sparse and scrub like. Small trees such as the native pine (*Pinus brutia*), juniper (*Juniperus phoenicea*) and  
105 olives (*Olea europea*), Carob (*Ceratonea siliqua*) are interspersed amidst low lying bushes such as *Inula viscosa* and *Foeniculum vulgare*. In addition small groves of vines, almonds and pomegranates are kept by some local farmers. In summer, Cyprus is normally influenced by the Etesian winds, which bring air masses from the north (from Eastern Europe, and crossing Turkey and Greece). However, in 2014 a southward displacement of the storm track and associated synoptic weather  
110 systems weakened the east-west pressure gradient (Tyrlis et al., 2015) delaying the onset of the Etesian winds and causing periodic influence of air advected from the West over the Mediterranean Sea. Despite clear variation in air mass origin during this campaign (12 July–03 August 2014) the local wind direction at the site was primarily SW (72%, see Fig. 1).

### 2.2 Instrumentation

115 Measurement instruments were installed in four air-conditioned laboratory containers, positioned in two stacks of two with a 8 m tall, 0.5 m diameter, high flow (10 m<sup>3</sup> min<sup>-1</sup>) common inlet situated between the stacks (see Fig.1). The common inlet was designed to minimize wall losses of species in air drawn from the 8 m high sampling point, and to avoid small scale measurement differences caused by individual inlet positioning. For the measurement of VOCs a slower subsample flow (5 L min<sup>-1</sup>)  
120 was drawn through insulated and heated (35 °C) Teflon lines (OD = 1.27 cm) installed perpendicular to the direction of main inlet flow and into the VOC group measurement container. This air was analyzed by a Proton Transfer Reaction Time Of Flight Mass Spectrometer (PTR-TOF-MS), an OH reactivity system, two Gas Chromatography systems with a Flame Ionization Detector (GC-FID) and one Gas Chromatography system combined with a Mass Spectrometer (GC-MS).

<sup>2</sup>[http://www.populationlist.com/Eparchia\\_Pafou/06/760931/state-population](http://www.populationlist.com/Eparchia_Pafou/06/760931/state-population); accessed on 16 August 2016



## 125 2.2.1 Proton Transfer Reaction Time of Flight Mass Spectrometer

On-line VOC measurements were performed with a PTR-TOF-MS (Ionicon Analytik GmbH, Innsbruck, Austria). This instrument has been described in detail elsewhere (Graus et al., 2010; Veres et al., 2013). Post-acquisition data analysis was performed using the program “PTR-TOF DATA ANALYZER”, which is detailed elsewhere (Müller et al., 2013). The time resolution of the measurements was 1 min and the background level was determined every two hours for twenty minutes by passing air through a catalytic converter containing platinum coated pellets heated to 320 °C. The drift pressure was maintained at 2.20 mbar and the drift voltage 600 V (E/N 137 Td). To perform mass scale calibration 1,3,5-trichlorobenzene was permanently bled into the sample stream as an internal standard. A comprehensive 4 point humidity dependent calibration of the instrument was performed at the beginning and at the end of the campaign using a commercial gas standard (Apel-Riemer Environmental) containing 14 compounds. The sensitivity of the instrument, which was interpolated linearly over the campaign and is expressed in normalized counts per second per ppbv (ncps ppbv<sup>-1</sup>), decreased by a range of 0.6 ncps ppbv<sup>-1</sup> (e.g. isoprene) to 3 ncps ppbv<sup>-1</sup> (e.g. methanol).

140 With increasing humidity the sensitivity decreased exponentially for most of the species. Only isoprene and methanol did not show any humidity dependency. Calibration factors were applied by taking the time of the measurement as well as the humidity for each data point into account. Detection limits for each species quantified were determined by calculating three times the standard deviation of the background measurement. The results lay between 15 pptv (e.g. acetonitrile) and 200 pptv (methanol). The total uncertainty is defined by the statistical error, which was calculated from the geometric combination of the noise, and the systematic error. The latter contains the error of the calibration, the flow measurements, the calibration gas bottle accuracy as well as the maximum error occurring due to changes in sensitivity. The values of the total uncertainty varied between 10 and 15 %. Only methanol had a higher total uncertainty of 30 % due to problems during calibration.

150 Acetic acid was calibrated separately by the use of a permeation source, because it was not included in the pressurized gas standard. For the acid only one calibration was performed in the field with two different humidities. As found by Feilberg et al. (2012) the humidity dependency of acetic acid shows a linear behavior. After the campaign a second calibration was done in the laboratory at three different humidities. The calibration factors obtained in the field and in the laboratory differed by a factor of ca. 2.5. Also the slope of the linear interpolations between the calibration factors of different humidities measured in the laboratory and in the field varied. Therefore the fit parameters of both linear regressions were averaged and the resulting mean fit function was used to calculate the calibration factor according to the humidity at the time. The discrepancy in the calibration factors leads to a high total uncertainty of 47%.

160 Acetic acid was measured at mass 61.0284 amu, but its mixing ratios must be considered as upper limits, because the PTR-TOF-MS is not able to distinguish between acetic acid and its isomer



glycolaldehyde (Baasandorj et al., 2014). Furthermore, fragments of peroxyacetic acid (PAA) and ethyl acetate can also be measured on the exact mass of acetic acid (Baasandorj et al., 2014). However, since the sources of ethyl acetate are mainly anthropogenic and the measurement site remote,  
165 we assume that the influence of ethyl acetate was negligible. This assumption is supported by the finding that the signal at 61.0284 amu was significantly reduced during periods when the site was impacted by fog, indicating that the responsible trace gas was highly soluble in water. The potentially interfering molecule ethyl acetate is not nearly as soluble:  $0.059 \text{ mol m}^{-3} \text{ Pa}^{-1}$  in comparison to  $40\text{--}46 \text{ mol m}^{-3} \text{ Pa}^{-1}$  for acetic acid, see (Sander, 2015).

170 The PTR-TOF-MS was not calibrated for PAA and monitored it only during a few days of the campaign at mass 77.0233 amu. On these days the PAA signal in counts per second (cps) was very low (ca. 0.3 cps). Španěl et al. (2003) reported that 90 % of PAA are measured at the exact mass of acetic acid, while 10 % are recorded at the mass of the mother ion (77.0233 amu). If this is taken into account, PAA would still influence acetic acid only between 10 and 20 % because of the low count  
175 rates.

A Chemical Ionization Mass Spectrometer (CIMS) designed to measure PAA was operated in two modes during the campaign (Phillips et al., 2013). From  $\sim 17\text{--}24$  July the CIMS measured PAA only and found very low values, close to the detection limit. From  $\sim 26$  July until the end of the campaign the collisional dissociation parameters were adjusted and PAA and acetic acid were de-  
180 tected on the same mass (59 amu). It was only discovered after Cyphex that the CIMS measured not only PAA but also acetic acid, and the approximate, relative sensitivity to PAA and acetic acid was only determined a year later. For this reason, the absolute values for the CIMS data are highly uncertain, but reveal that PAA levels were substantially lower than those of acetic acid. Figure 2 displays the acetic acid and the PAA traces as well as their correlation and it can be seen that the PAA data  
185 without accompanying detection of acetic acid (blue line) showed very low values between 0 and 200 pptv from  $\sim 17\text{--}24$  July. The later period from  $\sim 26$  July until 3 August exhibited much higher signals due to the sum of PAA and acetic acid. The correlation in the CIMS and the PTR-TOF-MS time profiles with a correlation factor of 0.74 suggests that most of this is due to acetic acid. The potential interference in the PTR-TOF-MS signal for acetic acid is thus small compared to the 47%  
190 total uncertainty of the acetic acid measurements.

The main sources of glycolaldehyde, which is an isomer of acetic acid and can therefore not be distinguished from the acetic acid signal, are biomass burning and secondary production from isoprene and ethene degradation (Niki et al., 1981; Paulson and Seinfeld, 1992). Since the acetonitrile levels stayed low during the whole campaign we can exclude a significant influence of biomass burning.

195 Furthermore, as will be shown in the results section, isoprene levels were low due to the scarce vegetation and low local anthropogenic emissions occurred. The atmospheric lifetime of glycolaldehyde was calculated taking the removal by OH and photolysis into account. During the campaign an average OH concentration of  $\sim 2 \times 10^6 \text{ molec cm}^{-3}$  and an average photolysis rate of  $\sim 3 \times 10^{-6} \text{ s}^{-1}$



were determined. Using a reaction rate of  $8.0 \times 10^{-12} \text{ cm}^3 \text{ molec}^{-1} \text{ s}^{-1}$  provided by IUPAC (Atkinson  
200 et al., 2006) a lifetime of  $\sim 15$  h was calculated. Wet and dry deposition were not considered in  
this calculation and would reduce the lifetime even further. In most cases the air masses measured  
remained roughly 12 h to 5 days over the Mediterranean Sea before reaching Cyprus. This would  
mean that some glycolaldehyde could survive transport, especially during night, but the amount is  
expected to be small. Since there is no known ocean source for glycolaldehyde, we can assume that  
205 this compound has only a minor effect on the acetic acid signal. In view of the discussion above, the  
acetic acid mixing ratios shown in the following analysis may be regarded as an upper limit.

### 2.2.2 Monoterpenes, ozone, CO and meteorological parameters

Monoterpenes were measured by a commercial GC-MS system (MSD 5973; Agilent Technologies  
GmbH) combined with an air sampler and a thermal desorber unit (Markes International GmbH) and  
210 the sample interval was 45 min.

Ozone was monitored using a U.V. Photometric  $\text{O}_3$ -Analyzer (model 49, Thermo Environmental  
Instruments, U.S.) The detection limit was 2 ppbv and the overall uncertainty less than 5 %.

CO was measured by a Room Temperature Quantum Cascade Laser (RT-QCL) (Li et al., 2012). The  
instrument uses wavelength modulation absorption spectroscopy ( $2190 \text{ cm}^{-1}$ ) over a path length of  
215 36 m to measure CO at a time resolution of 1 s. The detection limit was determined to be 0.4 ppbv  
and the overall uncertainty 14.4 %. For more information please refer to Li et al. (2012).

The weather station Vantage Pro2 (Davis Instruments Corp., Hayward, CA) was used to measure  
temperature, pressure, wind direction and speed, solar radiation and humidity with a time resolution  
of 1 minute.

## 220 2.3 Modeling

### 2.3.1 FLEXPART model

The dynamical transport history of air reaching Cyprus during the CYPHEX campaign was deter-  
mined by using the Lagrangian particle dispersion model FLEXPART (Stohl et al., 2002, 2005,  
2007). It computes trajectories of infinitesimally small air parcels (so-called particles) to describe  
225 the transport and diffusion of tracers (Stohl et al., 2005). Thereby mean winds interpolated from  
analysis fields and turbulence represented by random motions are used (Stohl et al., 2007).

In this study, FLEXPART was run backward in time from the measurement site driven with analyses  
from the ECMWF with  $0.2^\circ \times 0.2^\circ$  horizontal resolution (derived from T799 spectral truncation),  
a vertical resolution of 137 model levels and temporal resolution of 1 h, which was a combination  
230 of 6 h analyses and short-term forecasts. Backward simulations were made for 3 h time intervals be-  
tween 12 July 2014 and 03 August 2014 and for each interval 10000 passive air tracer particles were  
released and followed backward in time for 120 h. The distribution of tracer particles was analyzed



during the 120 h simulation and led to a particle density distribution describing the residence time in each cell of a defined geographical grid. Column-time integration of residence times resulted in  
235 a horizontal distribution indicating the total upwind area of influence. Regions of higher residence times during the simulation period identified major transport routes of air reaching the site.

### 2.3.2 CAABA/MECCA

To investigate photochemical processing over the ocean, the observations were compared to simulations with the chemical box model CAABA/MECCA (Sander et al., 2011). We used version 3.8,  
240 which includes the recently developed comprehensive organic reaction scheme MOM (Mainz Organics Mechanism) by Lelieveld et al. (2016). Focusing on organics, we switched off halogen and sulfur chemistry, as well as heterogeneous and aqueous phase reactions in view of the low cloudiness and aerosol concentrations. Initial values based on the EMAC model (Jöckel et al., 2016) are available in the supplement together with a complete list of chemical reactions used in this study,  
245 rate coefficients and references. Photolysis rate constants were calculated for the latitude of Cyprus. The model simulated a period of two days, starting on 19 July at 6 am. No further emissions were injected during the model run, except ozone to simulate its entrainment from the free troposphere into the boundary layer. Dry deposition as well as uptake by aerosols were not considered in this study. The results will be discussed in section 3.2.2.

## 250 3 Results

### 3.1 Biogenic compounds

In general, the mixing ratios of biogenic compounds measured at the site were low, with the sum of isoprene (m/z 69.0699 amu) and monoterpenes (m/z 137.1325 amu) never exceeding 0.5 ppbv and a campaign average daily maximum of  $\sim 0.1$  ppbv for both. This is in contrast to tropical forest regions  
255 where typical values of 8 ppbv isoprene have been reported recently (Yañez Serrano et al., 2014), but consistent with levels reported from the Mediterranean areas (Liakakou et al., 2007; Davison et al., 2009). Comparable emission rates of isoprene and the sum of monoterpenes can be regarded as typical for the Mediterranean vegetation (Kesselmeier and Staudt, 1999). Since both isoprene and monoterpenes have atmospheric lifetimes on the order of minutes to hours with respect to the removal by OH, we concluded that they must have been emitted by local vegetation. Figure 3 displays  
260 the campaign averaged, diel cycles of the sum of the monoterpenes and of isoprene. Both median diel cycles follow a roughly sinusoidal curve and were strongly light dependent. This finding is consistent with the literature concerning isoprene and monoterpene emissions and atmospheric mixing ratios in the Mediterranean area (Kesselmeier et al., 1998; Liakakou et al., 2007; Davison et al.,  
265 2009).

Figure 4 shows the course of isoprene and the main monoterpene species as observed over the



whole campaign detected by a GC-MS system with  $\alpha$ -pinene being the dominant species among the monoterpenes quantified. At night the values were close to the detection limit of the PTR-TOF-MS, but the GC-MS data revealed that the mixing ratios of isoprene and monoterpenes decreased to  
270 nearly zero in almost all nights (see Figure 4). This light dependent behavior of the monoterpenes indicates that the vegetation is dominated by broad leaf species. Conifers, on the other hand, are able to store specific monoterpenes and emit them also depending only on temperature or other stress (Kesselmeier and Staudt, 1999, and references therein) so that elevated levels could also be found at night (e.g. Davison et al., 2009; Staudt et al., 1997).

275 The mean isoprene mixing ratios (Fig. 3) show slightly elevated values in comparison to the median values in the morning and afternoon. A potential explanation can be found by considering the changes in meteorological conditions during these parts of the day, e.g. variation of the local boundary layer height relative to the hilltop site or the onset of the local sea breeze. The impact of these changes varied during the campaign, potentially causing the difference between median and mean  
280 values and motivates a closer look to single days. To exemplify this, isoprene from 22 July has been plotted at 1 minute time resolution (Fig. 5). On that day at around 9:30 am local time the wind changed from N-NE to W-SW direction as accompanied by a sharp increase in relative humidity and in atmospheric dimethylsulfide (DMS), a species primarily emitted from marine sources (Cline and Bates, 1983; Mesarchaki et al., 2014). Before the wind direction changed, isoprene initially in-  
285 creased together with temperature. But as soon as the wind came from a region where the distance between ocean and site was shorter, isoprene levels decreased rapidly. This behavior is consistent with the current understanding that the sea is only a weak source of isoprene and the main source is the local terrestrial vegetation (Bonsang et al., 1992; Broadgate et al., 1997; Palmer and Shaw, 2005; Arnold et al., 2009). However, isoprene did not always follow this pattern. On occasions isoprene  
290 levels stayed elevated in the morning despite a drop in temperature and associated increase in relative humidity and DMS. One explanation for this is an influence from a small forest upwind of the site. The Pikni forest 7 km to the southwest and some 300 m lower than the site can, given the right meteorological conditions, contribute to isoprene levels at the site despite its short lifetime (ca. 30 minutes with respect to the removal by OH, using a mean OH concentration of  $5 \times 10^6$  molec  $\text{cm}^{-3}$   
295 measured between 6 am and 10 am). With an assumed average wind speed of 3.5 m/s the transport time of isoprene from the forest to the site would amount to  $\sim 30$  minutes. The same reasoning can be applied to the monoterpenes, because their lifetime amounts to ca. 60 min. with respect to the removal by OH (calculated for  $\alpha$ -pinene and an OH concentration of  $5 \times 10^6$  molec  $\text{cm}^{-3}$ ). But in contrast to the isoprene data, the median and mean mixing ratios of the total monoterpenes showed  
300 less discrepancy, which might indicate differences concerning the source behavior. One possible explanation could be that species with different emission patterns for isoprene and for monoterpenes were not co-located. If the Pikni forest for example would be dominated by isoprene emitting plants, its irregular influence on the site could cause discrepancies between median and mean values of iso-



prene while the monoterpenes would remain unaffected. Other reasons supposedly exist, such as a  
305 different emission regulation. However, direct measurements to demonstrate such different primary  
emissions were not performed and the atmospheric concentration development indicates a clear light  
dependent emission regulation for monoterpenes as for isoprene with a very close relationship be-  
tween isoprene and monoterpene production.

In summary, the local vegetation produces modest emissions of reactive isoprene and monoterpenes.  
310 Their diel mixing ratio profiles are both light driven with a maximum around midday and slight  
variations can be traced back to changes in the local meteorology.

### 3.2 Oxygenated volatile organic compounds (OVOCs)

#### 3.2.1 Local impacts and transport processes

In contrast to the pronounced diel cycles and low mixing ratios found for the biogenic compounds  
315 the oxygenated VOCs showed relatively high values with comparatively little variation. Fig. 6  
displays the mean diel cycles of acetone, methanol and acetic acid. It becomes clear that the mean and  
median mixing ratios deviate in the morning and afternoon as already discussed for isoprene. The  
same reasoning is likely to apply: variable local meteorology leading to high values in the morning  
and afternoon on some days.

320 Methanol exhibited a maximum mean and median mixing ratio in the early morning. Since vegeta-  
tion is an important source of methanol under light conditions (Fall and Benson, 1996; Hüve et al.,  
2007) this increase could be explained by sunlight dependent plant emissions or by evaporation of  
methanol collected in dew. However, the production and emissions processes in plants are a matter  
of discussion (Folkers et al., 2008). The median mixing ratios of acetic acid indicate that a weak  
325 diel cycle is present. The acetic acid mixing ratios (humidity corrected) reveal a pronounced diel  
cycle between the 16 and 21 July, which is displayed in Fig. 7. In this part of the campaign a distinct  
anticorrelation between the acetic acid mixing ratios and humidity is apparent. Fog formation, which  
occurs under specific meteorological conditions, notably 100 % relative humidity (RH) in the pres-  
ence of cloud condensation nuclei, leads to droplet sedimentation, so that soluble gases are largely  
330 removed. Acetic acid is more strongly affected than acetone and methanol, because the latter are a  
factor 143 and 22 less soluble, respectively (Sander, 2015). Uptake to droplets and sedimentation  
only occurs when 100 % relative humidity is reached and thus cannot explain the diel cycle of acetic  
acid at less than 100 % RH. Three other effects could play a role in this process: first, local photo-  
chemical production of acetic acid, second, in-mixing from the free troposphere by turbulence and  
335 third, emission from and/or uptake by vegetation and soil. The measured production from 06:00 till  
14:00 and the loss rate from 14:00 till 22:00 during the period from the 16 to the 21 July amounted  
roughly to 0.1 ppbv/h and 0.08 ppbv/h, respectively. Sanhueza and Andreae (1991) reported a daily  
average emission of acetic acid from savanna soil of  $0.07 \text{ nmol m}^{-2} \text{ s}^{-1}$ . Assuming a planetary bound-



ary layer (PBL) height of 500 m this would give a production rate of 0.012 ppbv/h. Although a direct  
340 comparison might be difficult, because the measurements were performed at different locations, the  
discrepancy of one order of magnitude strongly indicates that other processes than emission from  
soil played a role. According to Paulot et al. (2011), emissions from terrestrial vegetation account  
for 3 % of the total sources while secondary photochemical production represents the major part of  
69 %. However, in a remote site the contribution of secondary production is expected to be minor due  
345 to a lack of precursors. Thus, it was concluded that in-mixing from the free troposphere contributed  
to the net, apparent production rate with the onset of turbulent mixing in the morning. It is assumed  
that, in comparison to the PBL, acetic acid levels are elevated in the free troposphere due to the high  
deposition rate of the acid within the PBL. The distinct diel cycles of acetic acid also coincided with  
a period of higher solar radiation (see Fig. 7), which promoted turbulence.

350 Hartmann et al. (1991) determined a dry deposition rate of 0.5–1 cm/s for acetic acid in a savanna re-  
gion. A boundary layer height of 500 m and an average acetic acid mixing ratio of 1 ppbv during the  
day would result in a loss rate of 0.04–0.07 ppbv/h. The measured loss rate in Cyprus (0.08 ppbv/h)  
was already quite close to these values, which suggests that dry deposition is the major loss process  
of acetic acid.

355 The reason why acetic acid did not display diel variability during the whole campaign is related to  
varying meteorological conditions, e.g. in the periods associated with strong decreases in humidity  
the site was likely within the free troposphere at night so that no distinct diel cycles could be estab-  
lished. Furthermore long distance transport could have dominated over local processes.

To investigate the influence of transport processes the source regions and transport pathways of air  
360 arriving at the site were examined using the FLEXPART model. The area of influence of each single  
simulation can be described by the fraction of time the air has spent over different regions. For  
this study, the upwind region, namely the European continent, has been delineated into color coded  
sections, see Fig. 8, upper left panel. Thus, the overall transport time for air masses reaching the site  
can be subdivided in specific colored fractions between 0 and 1. As one single colorbar character-  
365 izes the transport history of air at a certain time step, the combination of all colorbars of all single  
simulations weighted by time results in an overview of the evolution of transport patterns. This is  
shown in upper part of the right panel of Fig. 8.

The lower part of the right panel of Fig. 8 shows for each simulation the fraction of the time the air  
has spent within the planetary boundary layer, where surface processes (e.g. surface emissions or  
370 uptake of trace gases) can influence the air composition. This fraction lay between 10% and 35%.

To determine the footprint for a spatially and temporally variable layer as the PBL it was necessary  
to consider the PBL height over time at each single column within the area of influence. For exam-  
ple the air mass that arrived on 21 July in Cyprus had spent 30 % of the last 120 h within the PBL  
(see lower panel on the right in Fig. 8). Of these 30 %, two thirds were affected by Eastern Europe,  
375 marked in red, purple and pink. In contrast, on the 25 July the air was 35 % of the time inside the



PBL, whereof the main part was within marine boundary layer (MBL, marked in blue).

In the center section of the graph, mixing ratios of methanol, acetone and acetic acid are plotted on the same time scale. From Fig. 8 it can be seen that the mixing ratios of all three compounds were higher when the air sampled came from Eastern Europe (red, purple, pink) and lower when arriving  
380 from western areas (shades of green). Transport from the West to Cyprus entails longer transport times in the Mediterranean marine boundary layer than from the East. The trend implies that either the sources in Eastern Europe were stronger or removal processes had a greater influence in air transported from the West.

In Table 1 campaign averaged mixing ratios of different VOCs, O<sub>3</sub> and CO are listed and separated  
385 by Eastern and Western air flow. Consistent with methanol, acetone and acetic acid, other OVOCs like acetaldehyde and methylethylketone as well as O<sub>3</sub> and CO show higher mixing ratios in air masses with Eastern European origin. The mixing ratio of acetonitrile, a tracer for biomass burning, was ca. 110 pptv in both flow regimes. These low mixing ratios and the lack of variability indicates that no air masses influenced by recent biomass burning reached Cyprus in the period of measure-  
390 ment. Anthropogenic tracers, such as the aromatic compounds benzene, toluene and the xylenes, showed very low mixing ratios between 20 and 50 pptv, which confirms the remote location of the site and the minor influence of local anthropogenic emissions. This is also stressed by the small number of points which are above the detection limit (see Table 1). The high standard deviations of these aromatic compounds can be traced back to some rarely occurring spikes. The ozone mixing  
395 ratios of 60 - 70 ppbv are consistent with or even slightly higher than values found in Gerasopoulos et al. (2005) and Kleanthous et al. (2014). The values measured during CYPHEX also exceed the European Air Quality Standard of 120 µg m<sup>-3</sup> (60 ppbv as a maximum daily 8 h mean)<sup>3</sup>.

In the following section we examine the role of photochemical processes on the mixing ratios of the OVOCs.

### 400 3.2.2 Investigation of photochemical processes using the CAABA/MECCA box model

The CAABA/MECCA box model was used to examine the photochemical processes influencing the mixing ratios of acetone, acetic acid and methanol. In order to simulate conditions in the MBL, where no major sources can be found, only initial values of precursors were set, with further emissions during the run deactivated, except for ozone. Dry deposition was also excluded, because this  
405 model run was intended to investigate photochemistry only. The trace gases included, their initial values (which originate from the Mainz Organics Mechanism (MOM) chemistry in the EMAC model (Jöckel et al., 2016)) as well as the chemical degradation scheme can be found in the supplement. The model mixing ratios cannot be directly compared to the results of section 3.2.1, because processes like transport, ocean emission/uptake or dry deposition were not included in the box model.  
410 In Fig. 9 the predicted mixing ratios of methanol, acetone and acetic acid are displayed for a 48 h

<sup>3</sup><http://ec.europa.eu/environment/air/quality/standards.htm>; accessed 11 July 2016



model run with an initial value for NO<sub>x</sub> of 2.4 ppbv. While methanol and acetic acid decrease, the mixing ratio of acetone increases. Figures 10, 11 and 12 display the rates of important reactions with a production or loss rate  $\geq 10^{-16}$  mol mol<sup>-1</sup> s<sup>-1</sup> (0.36 pptv/h) impacting the budgets of the OVOCs. The main process affecting methanol is the degradation by OH radicals. For acetic acid, production  
415 via the peroxy acetyl radical (CH<sub>3</sub>C(O)O<sub>2</sub>) is countered by its loss via reaction with OH. Net production of acetic acid can be achieved only if enough organic precursors are emitted at low NO<sub>x</sub> level (ca. 300 pptv), which reduces the OH mixing ratio. The modeled behavior of acetone is more complex. Among the most important reactions are its loss by OH radical reaction or photolysis as well as its production via the reaction of different intermediates, mainly peroxy radicals, with NO or  
420 OH, for example the reaction of isopropyl peroxy radicals (iC<sub>3</sub>H<sub>7</sub>O<sub>2</sub>) with NO. It can be concluded that secondary production in the MBL plays only a role for acetone, while methanol and acetic acid are rather depleted.

### 3.2.3 Influence of marine boundary layer transport on OVOCs

In Fig. 13 mixing ratios of methanol, acetone, and acetic acid are plotted against the time the air  
425 spent in the marine boundary layer, calculated by adding up the FLEXPART modeled percentage of the influence of the Eastern and Western Mediterranean, the Black Sea, the Caspian Sea and the Atlantic Ocean. The summed percentage was then multiplied by the duration of the modeled backward trajectories (120 h). The data were separated into periods affected by Eastern and by Western Europe. The r<sup>2</sup> values vary from 0.2–0.5, but the slopes were consistently negative in all cases, and  
430 steeper for air masses from Eastern Europe. The OVOC loss rate values amounted to 0.1 ppbv/h for methanol, 0.06 ppbv/h for acetone and 0.05 ppbv/h for acetic acid for the Eastern outflow and 0.06 ppbv/h for methanol, 0.02 ppbv/h for acetone and 0.03 ppbv/h for acetic acid for a flow from the West. The net effect of transport over water for all three substances is a function of dilution (by vertical and horizontal mixing), photochemical degradation, uptake or emission by the ocean and  
435 production from the oxidation of larger organic molecules. As already mentioned the atmospheric lifetimes with respect to the removal by OH radicals were about 6 days for methanol, 32 days for acetone and 8 days for acetic acid. FLEXPART calculated transport times from Eastern Europe to Cyprus of roughly 12 h to 2 days and from Western Europe to the site of around 2–5 days. Clearly the atmospheric lifetimes of acetone, methanol and acetic acid are all relatively long compared to  
440 the average transport time. This allows the influence of the MBL to be gauged. Only acetic acid was impacted by local effects in the period from 16–21 July, shown by its diel cycle. Since this period coincides with an Eastern flow regime, only air masses from Western Europe were investigated in the following study. The loss rates of the three OVOCs were calculated using the subsequent formula:

$$[RH]_t = [RH]_0 \times \exp(-(k_{OH} \times [OH] + V_{dep}) \times t) \quad (1)$$



445 where  $[RH]_t$  is the mixing ratio of the compound at a specific transport time  $t$ ,  $[RH]_0$  the mixing  
ratio at the starting point of the linear fit,  $k_{OH}$  the rate coefficient for the reaction with OH radicals,  
 $[OH]$  the concentration of the OH radicals and  $V_{dep}$  the dry deposition rate. Photolysis rates are so  
low that they can be neglected. The diel averaged  $[OH]$  mixing ratio at the site was measured during  
the CYPHEX campaign as  $2 \times 10^6$  molec  $cm^{-3}$ .  $k_{OH}$  values originate from IUPAC (Atkinson et al.,  
450 2006). Since OH concentrations were constrained by measurement and the OH rate coefficients are  
well known this loss term is assumed to be reasonably accurate. Dry deposition rates, on the other  
hand, represent a large uncertainty factor and dilution by vertical and horizontal mixing is not ac-  
counted for in the equation. Three different scenarios are considered here:

455 1. Dry deposition rates simulated in EMAC (Jöckel et al., 2016) over the Mediterranean sea were  
taken and amounted to  $0.41$   $cm\ s^{-1}$  for acetic acid,  $0.031$   $cm\ s^{-1}$  for acetone and  $0$   $cm\ s^{-1}$  for  
methanol despite the higher solubility of methanol in comparison to acetone. The values are  
net deposition velocities calculated in a resistant-type scheme, so they may not proportionate  
the solubilities of the species. An average PBL height of  $500$  m was assumed. The results can  
460 be found as light blue lines in Fig. 13. The black lines represent the linear fit of the measured  
data. It becomes clear that acetic acid is well captured by the calculation while the measured  
net loss was greater than the calculated loss for methanol and acetone.

465 2. In the second scenario dry deposition rates were adjusted so that the measured loss rates  
were reached. This method yielded a dry deposition rate constant of  $0.21$   $cm\ s^{-1}$  for methanol,  
 $0.10$   $cm\ s^{-1}$  for acetone and  $0.42$   $cm\ s^{-1}$  for acetic acid, still assuming a PBL height of  $500$  m.  
These values do not reflect the relative solubilities. According to Sander (2015) methanol  
has a Henry's Law constant between  $1.7$  and  $2.2$   $mol\ m^{-3}\ Pa^{-1}$ , acetone between  $0.26$  and  
 $0.33$   $mol\ m^{-3}\ Pa^{-1}$  and acetic acid between  $40$  and  $46$   $mol\ m^{-3}\ Pa^{-1}$ . Based on solubility alone  
we would therefore expect the acetic acid loss rate to be much higher than that of acetone.

470 3. In the last scenario the dry deposition of methanol was adjusted so that the loss rate matches  
the measured one ( $0.21$   $cm\ s^{-1}$ ). The dry deposition rates of acetic acid and acetone were set  
according to their relative solubilities:  $4.4$   $cm\ s^{-1}$  for acetic acid and  $0.031$   $cm\ s^{-1}$  for acetone.  
The results can be found as violet lines in Fig. 13. Interestingly the value for acetone gained  
by this method is the same as in the model and its loss rate is still underestimated. The loss  
475 rate of acetic acid is now even higher than the measured one.

Clearly, the measured loss rates of methanol and acetone are higher than expected. Although the  
acetic acid loss rate is nicely reproduced by the model, a higher loss rate would be anticipated owing  
to its solubility. Four possible explanations for this apparent anomaly will be considered here. The  
first is that vertical transport to the sea surface layer was a limiting factor, so that turbulence rather  
480 than solubility defined the distribution. The second is that sea-water surface layer concentrations



of acetic acid were high relative to methanol and acetone, compensating for the difference in solubilities. The third is that photochemical production of acetic acid in air was much more influential than that of acetone and methanol. The fourth is that in-mixing of air from the free troposphere is significant.

485 A turbulence driven distribution can be the reason why the loss rates do not represent the solubilities of the three OVOCs, but it cannot explain the discrepancy between the measured and the calculated loss rates of methanol and acetone. Other explanations need to be consulted.

Although ocean concentrations and air-sea fluxes of acetone and methanol have been determined previously (Williams et al., 2004; Sinha et al., 2007), to our knowledge no equivalent measurements  
490 for acetic acid exist. Generally it has been found for methanol and acetone that the ocean and air are close to equilibrium on a global scale (Millet et al., 2008; Fischer et al., 2012), but that a significant aqueous phase production term exists for both species. Regionally, strong biological activity can drive a surface ocean oversaturation of acetone that leads to its emission (Taddei et al., 2009). Dixon et al. (2014) have shown that methanol is more efficiently consumed microbially than acetone. One  
495 reason for the higher loss rate of methanol in comparison to acetone could therefore be the higher oxidation rate of methanol in the ocean.

Significant in-situ photochemical production would also lead to an underestimation of loss rates. Estimates of global budgets of the three OVOCs reveal that photochemical production is larger for acetic acid relative to methanol and acetone (Millet et al., 2008; Paulot et al., 2011; Fischer et al.,  
500 2012). However, the CAABA/MECCA box model indicates that acetic acid is depleted over the ocean rather than produced due to a lack of precursors (see section 3.2.2). The model results for acetone on the other hand showed a slight production. Therefore, photochemical production would increase the discrepancy between observed and expected loss rates for acetic acid and for acetone.

Another possible reason for the high loss rates could be in-mixing of acetone and methanol poor  
505 air from the free troposphere. That in-mixing took place or that the site was even within the free troposphere is confirmed by strong decreases in humidity levels (see Fig. 7) and by the loss rate of CO. In general no significant loss of CO is assumed over the ocean due to its long lifetime of ca. 40 days with respect to the removal by OH and its negligible dry deposition. However, a loss rate of 0.65 ppbv/h, which is higher than expected, was determined. Thus, it can be concluded that entrain-  
510 ment of air from the free troposphere occurred. If dry deposition rates reflecting the solubilities are assumed, it would therefore mean that acetic acid rich air caused a reduction in its net loss rate. As discussed above, a higher mixing ratio of acetic acid in the free troposphere is reasonable due to its high deposition loss rate in the PBL.

The most likely explanation for our observations are that vertical entrainment impacted on the mix-  
515 ing ratios measured downwind of the source regions. Furthermore microbial consumption within the sea surface layer could play a role.



### 3.2.4 Correlations between acetone, methanol, acetic acid, CO and ozone

Table 2 shows slopes, intercepts and correlation coefficients ( $r^2$ ) from the bivariate fits between methanol, acetone, acetic acid, CO and ozone separated by eastern and western air masses. In the  
520 acetone data the two spikes occurring at the 24 July and 2 August were removed, because they were most probably emerging from local sources. It can be seen that the correlations calculated from air masses originating in Eastern Europe are, on average, higher than the ones from Western Europe. As already mentioned horizontal or vertical dilution/ in-mixing, photochemical processes as well as emission or uptake by the ocean play important roles during transport. These effects can influence  
525 the various compounds to different degrees, so that divergent correlation factors are expected. Figure 14 displays the correlations between the OVOCs divided into eastern and western flow regimes. The decreasing correlation factors appear as higher scatter between the trace-gases measured in western air masses. The highest correlation was found between acetone and acetic acid in the eastern flow ( $r^2=0.81$ ), while in the western flow the correlation between the same molecules, acetone and acetic  
530 acid, yields  $r^2=0.52$ , only. The slope between acetone and acetic acid on the other hand stayed almost the same for both flow regimes ( $\sim 1$ ). However, the graph referring to air coming from Western Europe shows two rather distinct branches. This can be understood if acetone and acetic acid were influenced by different loss and/or production processes that lead to the grouping of the data points along different correlation lines and the decreasing  $r^2$  value. The longer the transport time the more  
535 important are the discrepancies between loss and production. To a lesser degree, similar effects are found in the correlation between methanol and acetone. Here the correlation factors decreased from 0.76 (eastern flow) to 0.62 (western flow).

In Figure 15 correlations between methanol and acetone as well as acetic acid from western flow regimes are color coded by relative humidity and  $O_3$ . The methanol vs. acetone as well as acetic acid  
540 vs. acetone plots color coded by RH reveal that the origin of the different branches is tied into high relative humidity and thus fog events ( $RH > 90\%$ , black dots). Since methanol and acetic acid are more soluble than acetone, these compounds are more efficiently removed by droplet sedimentation in foggy conditions. This leads to a decrease in the slope and therefore the formation of the lowest branch.

545 Furthermore, the acetic acid vs. acetone plot color coded by  $O_3$  shows that higher ozone levels were correlated with higher acetic acid and/or lower acetone mixing ratios. The branching was most probably dominated by the relationship between acetic acid and ozone, because there was no correlation between acetone and ozone in the western flow regime ( $r^2=0.04$ ). Since ozone is in general generated by photochemical processes, the correlation may indicate that acetic acid is also generated  
550 photochemically, which would however contrast the conclusions of the box-model study (see section 3.2.2) in which acetic acid is lost rather than formed over the ocean due to a lack of precursors. Another reason for the correlation could be in-mixing of both compounds from the free troposphere as both acetic acid and  $O_3$  mixing ratios are expected to decrease close to the ground due to dry de-



position. Another indication for the impact of air masses from the free troposphere is the low relative  
555 humidity. The high ozone mixing ratios (color coded in yellow) coincide with RH levels below 70 %  
(color coded in blue), which can be interpreted that rather dry, but ozone rich air was influencing the  
site.

The correlation coefficients between acetic acid and methanol, listed in Table 2, showed no differ-  
ence between eastern and western air masses, but the slope slightly decreased when changing from  
560 eastern to western flow regimes. If only the loss rates over the ocean are taken into account (see Fig.  
13 and section 3.2.3) an increasing instead of decreasing slope would be expected, because acetic  
acid showed a weaker decline than methanol. The slope between methanol and acetone on the other  
hand increased when changing from eastern to western air masses, although a decrease would be  
expected. But the slopes are in general dominated by high values originating from air masses that  
565 stayed a comparatively short time in the MBL. Hence, other effects played an important role, e.g.  
different emission ratios on the continent, local impacts like fog events or changing meteorological  
conditions. Especially acetic acid was biased by these local effects during an eastern flow regime  
which can be seen in the diel cycles between the 16 and 21 July (see section 3.2.1).

Comparing the three OVOCs to CO (Table 2) shows that the slope as well as the correlation between  
570 methanol and CO remained remarkably constant between the western and eastern flow regimes  
(slope=0.067 and 0.065,  $r^2=0.44$  and  $0.45$ , respectively). In contrast to acetic acid and acetone, this  
correlation appears to be insensitive to the combined processes of dilution, marine uptake/emission  
and photochemical ageing for air masses in this region. The data can be compared to the MINOS  
campaign, which took place in Finokalia, Crete (Salisbury et al., 2003). One part of the MINOS  
575 campaign, with no biomass burning influence and an eastern flow regime (“period 1”), was the most  
appropriate to compare to the CYPHEX data. Interestingly, the ratio between methanol and CO cal-  
culated from Salisbury et al., (2003) (0.02 for “period 1”) is smaller than the one determined in this  
study (0.033). The reason for this is a lower CO mixing ratio (MINOS: 167 ppbv, CYPHEX: 107  
ppbv), while the methanol values were similar in both campaigns (MINOS: 3.34 ppbv, CYPHEX:  
580 3.54 ppbv). In the same way, the acetone/CO ratio measured in this study (0.025) for easterly con-  
ditions was larger than the one reported by Salisbury et al., (2003) (0.017, “period 1”) due to lower  
CO mixing ratios. The decreased CO values might be traced back to the economic crisis in Greece,  
which led to a reduction of industrial production and therefore to decreasing emissions of anthro-  
pogenic compounds like CO. Another interesting relationship arose between ozone and the OVOCs.  
585 Regarding western air masses the correlations between the OVOCs and ozone were extremely poor,  
the best being between acetic acid and  $O_3$  ( $r^2=0.25$ ), while the others were below  $r^2=0.01$ . In east-  
ern flow regimes, on the other hand, the correlations were slightly stronger. If the correlation plots  
among the OVOCs from eastern air masses are color coded by ozone (Fig. 16), it can be seen that  
all plots show the same pattern: the higher the ozone values the higher the OVOC mixing ratios.  
590 This can be explained by the shorter distance from Cyprus to the sources in Eastern Europe. Still,



it needs to be kept in mind that the sources for the four compounds are different, e.g. methanol is mainly biogenically produced while secondary photochemical production dominates for acetic acid over land. The reason for the correlation could simply be that the sources were co-located on the continent and due to the shorter transport time from Eastern Europe the various loss and production  
595 processes had a weaker impact than in air masses from Western Europe.

#### 4 Conclusions

During the 2014 CYPHEX campaign, air masses from Eastern (67 % of the time) and Western Europe (33 % of the time) were measured. Since the transport routes of the air pass over the Mediterranean Sea the impact of the marine boundary layer on VOCs and especially OVOCs could be  
600 investigated. Due to the sparse vegetation local biogenic emissions of isoprene and monoterpenes were weak (always <350 pptv). These species showed typical diel cycles with the highest mixing ratios around midday. The difference in median and mean mixing ratios in the isoprene data could be explained by the boundary layer evolution, the onset of a local sea breeze system and the presence upwind of a small forest in the southwesterly wind direction. The methanol and acetone mixing  
605 ratios revealed relatively little diel variation, but higher absolute mixing ratios, indicating that local emission or production was less significant in comparison to long range transport. Only acetic acid followed a pronounced diel cycle during one period of the campaign, which is the result of various local effects like emission from soil, in-mixing from the free troposphere due to turbulence as well as dry and wet deposition over land. The lack of diel cycles during the rest of the campaign can  
610 be explained by a higher impact of transport processes and different meteorological conditions. To exclude these local phenomena only data measured from western air masses were used to investigate the influence of the MBL during transport. The methanol, acetone and acetic acid data showed that uptake to the sea surface was not defined solely by solubility and that vertical entrainment likely played an important role. The correlation coefficients between the OVOCs were higher in eastern  
615 than in western air masses, which can be explained by the longer transport time over the ocean and thus stronger impacts of different production and loss processes in the western flow regime as well as some local effects like fog formation. The ratios of methanol/CO and acetone/CO were higher in this work than in a study performed over a decade ago, consistent with the lowering in the regional sources of CO. The results displayed here indicate that air reaching Cyprus from Eastern and  
620 Western Europe showed different OVOC characteristics due to different emission patterns, transport times as well as varying impact of photochemical processes, dilution and ocean uptake or emission.



#### Author contribution

B. Derstroff performed the PTR-TOF-MS measurements and prepared the manuscript with contribu-  
tions from J. Williams, J. N. Crowley, H. Fischer, J. Kesselmeier and the other co-authors. I. Hüser  
625 and H. Harder provided the data of the FLEXPART model, R. Sander instructed the application of  
the CAABA/MECCA box model. CO and ozone measurements were performed by U. Parchatka and  
monoterpene measurements by E. Bourtsoukidis. Peracetic acid data were provided by G. J. Phillips  
and J. N. Crowley, photolysis rates by J. Schuladen, dry deposition rates from the EMAC model  
by S. Gromov and OH concentrations by C. Mallik and H. Harder. J. N. Crowley and J. Lelieveld  
630 designed the study. C. Sauvage, C. Stönnner, A. Novelli, L. Tomsche and M. Martinez carried mea-  
surements out in Cyprus.

The authors declare that they have no conflict of interest.

#### 635 Data availability

The data set is available from the CYPHEX server on request. If desired, please send an email to  
jonathan.williams@mpic.de



*Acknowledgements.* We would like to thank our engineers Thomas Klüpfel and Rolf Hofmann for their help and support. Furthermore we thank the Cyprus Ministry of Defense for the use of the base of the National Guard  
640 at Ineia and the generous assistance of the Lara Naval Observatory staff. Our thanks also go to the Department of Labor Inspection for helping us set up the campaign. Additionally we would like to thank Laurens Ganzeveld for inspiring discussions.



## References

- European Commission, <http://ec.europa.eu/environment/air/quality/standards.htm>, accessed 11 July 2016.
- 645 Populationlist, [http://www.populationlist.com/Eparchia\\_Pafou/06/760931/state/T1textendashpopulation](http://www.populationlist.com/Eparchia_Pafou/06/760931/state/T1textendashpopulation), accessed on 16 August 2016.
- Worldbank, <http://data.worldbank.org/country/cyprus>, accessed on 4 May 2016.
- Arnold, S. R., Spracklen, D. V., Williams, J., Yassaa, N., Sciare, J., Bonsang, B., Gros, V., Peeken, I., Lewis, A. C., Alvain, S., and Moulin, C.: Evaluation of the global oceanic isoprene source and its impacts on marine organic carbon aerosol, *Atmos. Chem. Phys.*, 9, 1253–1262, doi:10.5194/acp-9-1253-2009, <http://www.atmos-chem-phys.net/9/1253/2009/>, 2009.
- 650 Atkinson, R.: Gas-phase tropospheric chemistry of organic compounds: A review, *Atmos. Environ.*, 24, 1–41, doi:10.1016/0960-1686(90)90438-S, <http://www.sciencedirect.com/science/article/pii/096016869090438S>, 1990.
- 655 Atkinson, R., Baulch, D. L., Cox, R. A., Crowley, J. N., Hampson, R. F., Hynes, R. G., Jenkin, M. E., Rossi, M. J., Troe, J., and Subcommittee, I.: Evaluated kinetic and photochemical data for atmospheric chemistry: Volume II - gas phase reactions of organic species, *Atmos. Chem. Phys.*, 6, 3625–4055, doi:10.5194/acp-6-3625-2006, <http://www.atmos-chem-phys.net/6/3625/2006/>, IUPAC Task Group on Atmospheric Chemical Kinetic Data Evaluation, <http://iupac.pole-ether.fr>, accessed on 12 July 2016, 2006.
- 660 Baasandorj, M., Millet, D. B., Hu, L., Mitroo, D., and Williams, B. J.: Measuring acetic and formic acid by proton transfer reaction-mass spectrometry: sensitivity, humidity dependence, and quantifying interferences, *Atmos. Meas. Tech. Discuss.*, 7, 10883–10930, doi:10.5194/amtd-7-10883-2014, <http://www.atmos-meas-tech-discuss.net/7/10883/2014/>, 2014.
- Bonsang, B., Polle, C., and Lambert, G.: Evidence for marine production of isoprene, *Geophys. Res. Lett.*, 19, 1129–1132, doi:10.1029/92GL00083, <http://dx.doi.org/10.1029/92GL00083>, 1992.
- 665 Broadgate, W. J., Liss, P. S., and Penkett, S. A.: Seasonal emissions of isoprene and other reactive hydrocarbon gases from the ocean, *Geophys. Res. Lett.*, 24, 2675–2678, doi:10.1029/97GL02736, <http://dx.doi.org/10.1029/97GL02736>, 1997.
- Cline, J. D. and Bates, T. S.: Dimethyl sulfide in the Equatorial Pacific Ocean: A natural source of sulfur to the atmosphere, *Geophys. Res. Lett.*, 10, 949–952, doi:10.1029/GL010i010p00949, <http://dx.doi.org/10.1029/GL010i010p00949>, 1983.
- 670 Davison, B., Taipale, R., Langford, B., Misztal, P., Fares, S., Matteucci, G., Loreto, F., Cape, J. N., Rinne, J., and Hewitt, C. N.: Concentrations and fluxes of biogenic volatile organic compounds above a Mediterranean macchia ecosystem in western Italy, *Biogeosciences*, 6, 1655–1670, doi:10.5194/bg-6-1655-2009, <http://www.biogeosciences.net/6/1655/2009/>, 2009.
- Dixon, J. L., Beale, R., Sargeant, S. L., Tarran, G. A., and Nightingale, P. D.: Microbial acetone oxidation in coastal seawater, *Front. Microbiol.*, 5, doi:10.3389/fmicb.2014.00243, <http://doi.org/10.3389/fmicb.2014.00243>, 2014.
- 680 Doche, C., Dufour, G., Foret, G., Eremenko, M., Cuesta, J., Beekmann, M., and Kalabokas, P.: Summertime tropospheric-ozone variability over the Mediterranean basin observed with IASI, *Atmos. Chem. Phys.*, 14, 10589–10600, doi:10.5194/acp-14-10589-2014, <http://www.atmos-chem-phys.net/14/10589/2014/>, 2014.



- Fall, R. and Benson, A. A.: Leaf methanol — the simplest natural product from plants, *Trends Plant Sci.*, 1, 296 – 301, doi:10.1016/S1360-1385(96)88175-0, <http://www.sciencedirect.com/science/article/pii/S1360138596881750>, 1996.
- 685 Feilberg, A., Liu, D., Adamsen, A. P. S., Hansen, M. J., and Jonassen, K. E. N.: Odorant Emissions from Intensive Pig Production Measured by Online Proton-Transfer-Reaction Mass Spectrometry, *Environ. Sci. Technol.*, 44, 5894–5900, doi:10.1021/es100483s, <http://dx.doi.org/10.1021/es100483s>, 2010.
- Fischer, E. V., Jacob, D. J., Millet, D. B., Yantosca, R. M., and Mao, J.: The role of the ocean in the global atmospheric budget of acetone, *Geophys. Res. Lett.*, 39, doi:10.1029/2011GL050086, <http://dx.doi.org/10.1029/2011GL050086>, 2012.
- 690 1029/2011GL050086, 2012.
- Folkers, A., Hüve, K., Ammann, C., Dindorf, T., Kesselmeier, J., Kleist, E., Kuhn, U., Uerlings, R., and Wildt, J.: Methanol emissions from deciduous tree species: dependence on temperature and light intensity, *Plant Biology*, 10, 65–75, doi:10.1111/j.1438-8677.2007.00012.x, <http://dx.doi.org/10.1111/j.1438-8677.2007.00012.x>, 2008.
- 695 Galbally, I. and Kirstine, W.: The Production of Methanol by Flowering Plants and the Global Cycle of Methanol, *J. Atmos. Chem.*, 43, 195–229, doi:10.1023/A:1020684815474, <http://dx.doi.org/10.1023/A%3A1020684815474>, 2002.
- Gerasopoulos, E., Kouvarakis, G., Vrekoussis, M. and Kanakidou, M., and Mihalopoulos, N.: Ozone variability in the marine boundary layer of the eastern Mediterranean based on 7-year observations, *J. Geophys. Res.*, 700 110, doi:10.1029/2005JD005991, <http://dx.doi.org/10.1029/2005JD005991>, 2005.
- Graus, M., Müller, M., and Hansel, A.: High Resolution PTR-TOF: Quantification and Formula Confirmation of {VOC} in Real Time, *J. Am. Soc. Mass. Spectrom.*, 21, 1037–1044, doi:10.1016/j.jasms.2010.02.006, <http://www.sciencedirect.com/science/article/pii/S1044030510001005>, 2010.
- Hartmann, W. R., Santana, M., Hermoso, M., Andreae, M. O., and Sanhueza, E.: Diurnal cycles of formic and acetic acids in the northern part of the Guayana shield, Venezuela, *J. Atmos. Chem.*, 13, 63–72, doi:10.1007/BF00048100, <http://dx.doi.org/10.1007/BF00048100>, 1991.
- Holzinger, R., Williams, J., Salisbury, G., Klüpfel, T., de Reus, M., Traub, M., Crutzen, P. J., and Lelieveld, J.: Oxygenated compounds in aged biomass burning plumes over the Eastern Mediterranean: evidence for strong secondary production of methanol and acetone, *Atmos. Chem. Phys.*, 5, 39–46, doi:10.5194/acp-5-39-2005, <http://www.atmos-chem-phys.net/5/39/2005/>, 2005.
- 710 39-2005, <http://www.atmos-chem-phys.net/5/39/2005/>, 2005.
- Hüve, K., Christ, M. M., Kleist, E., Uerlings, R., Niinemets, Ü., Walter, A., and Wildt, J.: Simultaneous growth and emission measurements demonstrate an interactive control of methanol release by leaf expansion and stomata, *J. Exp. Bot.*, 58, 1783–1793, doi:10.1093/jxb/erm03, <http://jxb.oxfordjournals.org/content/early/2007/03/20/jxb.erm038>, 2007.
- 715 Jöckel, P., Tost, H., Pozzer, A., Kunze, M., Kirner, O., Brenninkmeijer, C. A. M., Brinkop, S., Cai, D. S., Dyroff, C., Eckstein, J., Frank, F., Garny, H., Gottschaldt, K.-D., Graf, P., Grewe, V., Kerkweg, A., Kern, B., Matthes, S., Mertens, M., Meul, S., Neumaier, M., Nützel, M., Oberländer-Hayn, S., Ruhnke, R., Runde, T., Sander, R., Scharffe, D., and Zahn, A.: Earth System Chemistry integrated Modelling (ESCiMo) with the Modular Earth Submodel System (MESSy) version 2.51, *Geosci. Model Dev.*, 9, 1153–1200, doi:10.5194/gmd-9-1153-2016, <http://www.geosci-model-dev.net/9/1153/2016/>, 2016.
- 720 1153-2016, <http://www.geosci-model-dev.net/9/1153/2016/>, 2016.



- Kalabokas, P., Mihalopoulos, N., Ellul, R., Kleanthous, S., and Repapis, C.: An investigation of the meteorological and photochemical factors influencing the background rural and marine surface ozone levels in the Central and Eastern Mediterranean, *Atmos. Environ.*, 42, 7894–7906, doi:10.1016/j.atmosenv.2008.07.009, <http://www.sciencedirect.com/science/article/pii/S1352231008006407>, 2008.
- 725 Kalabokas, P. D., Volz-Thomas, A., Brioude, J., Thouret, V., Cammas, J.-P., and Repapis, C. C.: Vertical ozone measurements in the troposphere over the Eastern Mediterranean and comparison with Central Europe, *Atmos. Chem. Phys.*, 7, 3783–3790, doi:10.5194/acp-7-3783-2007, <http://www.atmos-chem-phys.net/7/3783/2007/>, 2007.
- Kalabokas, P. D., Cammas, J.-P., Thouret, V., Volz-Thomas, A., Boulanger, D., and Repapis, C. C.: Examination of the atmospheric conditions associated with high and low summer ozone levels in the lower troposphere over the eastern Mediterranean, *Atmos. Chem. Phys.*, 13, 10339–10352, doi:10.5194/acp-13-10339-2013, <http://www.atmos-chem-phys.net/13/10339/2013/>, 2013.
- 730 Kesselmeier, J. and Staudt, M.: Biogenic Volatile Organic Compounds (VOC): An Overview on Emission, Physiology and Ecology, *J. Atmos. Chem.*, 33, 23–88, doi:10.1023/A:1006127516791, <http://dx.doi.org/10.1023/A%3A1006127516791>, 1999.
- 735 Kesselmeier, J., Schäfer, L., Ciccioli, P., Brancaleoni, E., Cecinato, A., Frattoni, M., Foster, P., Jacob, V., Denis, J., Fugit, J., Dutaur, L., and Torres, L.: Emission of monoterpenes and isoprene from a Mediterranean oak species *Quercus ilex* L. measured within the BEMA (Biogenic Emissions in the Mediterranean Area) project, *Atmos. Environ.*, 30, 1841–1850, doi:10.1016/1352-2310(95)00376-2, <http://www.sciencedirect.com/science/article/pii/S1352231095003762>, 1996.
- 740 Kesselmeier, J., Bode, K., Schäfer, L., Schebeske, G., Wolf, A., Brancaleoni, E., Cecinato, A., Ciccioli, P., Frattoni, M., Dutaur, L., Fugit, J. L., Simon, V., and Torres, L.: Simultaneous field measurements of terpene and isoprene emissions from two dominant Mediterranean oak species in relation to a North American species, *Atmos. Environ.*, 32, 1947–1953, doi:10.1016/S1352-2310(97)00500-1, <http://www.sciencedirect.com/science/article/pii/S1352231097005001>, 1998.
- 745 Kleanthous, S., Vrekoussis, M., Mihalopoulos, N., Kalabokas, P., and Lelieveld, J.: On the temporal and spatial variation of ozone in Cyprus, *Sci. total Environ.*, 476–477, 677–687, doi:10.1016/j.scitotenv.2013.12.101, <http://www.sciencedirect.com/science/article/pii/S0048969713015842>, 2014.
- Kourtidis, K., Zerefos, C., Rapsomanikis, S., Simeonov, V., Balis, D., Perros, P. E., Thompson, A. M., Witte, J., Calpini, B., Sharobiem, W. M., Papayannis, A., Mihalopoulos, N., and Drakou, R.: Regional levels of ozone in the troposphere over eastern Mediterranean, *J. Geophys. Res.*, 107, doi:10.1029/2000JD000140, <http://dx.doi.org/10.1029/2000JD000140>, 2002.
- 750 Kouvarakis, G., Vrekoussis, M., Mihalopoulos, N., Kourtidis, K., Rappenglueck, B., Gerasopoulos, E., and Zerefos, C.: Spatial and temporal variability of tropospheric ozone (O<sub>3</sub>) in the boundary layer above the Aegean Sea (eastern Mediterranean), *J. Geophys. Res.*, 107, doi:10.1029/2000JD000081, <http://dx.doi.org/10.1029/2000JD000081>, 2002.
- 755 Lelieveld, J., Berresheim, H., Borrmann, S., Crutzen, P. J., Dentener, F. J., Fischer, H., Feichter, J., Flatau, P. J., Heland, J., Holzinger, R., Kormann, R., Lawrence, M. G., Levin, Z., Markowicz, K. M., Mihalopoulos, N., Minikin, A., Ramanathan, V., de Reus, M., Roelofs, G. J., Scheeren, H. A., Sciare, J., Schlager, H., Schultz, M., Siegmund, P., Steil, B., Stephanou, E. G., Stier, P., Traub, M., Warneke, C.,
- 760



- Williams, J., and Ziereis, H.: Global Air Pollution Crossroads over the Mediterranean, *Science*, 298, 794–799, doi:10.1126/science.1075457, <http://dx.doi.org/10.1126/science.1075457>, 2002.
- Lelieveld, J., Gromov, S., Pozzer, A., and Taraborrelli, D.: Global tropospheric hydroxyl distribution, budget and reactivity, *Atmos. Chem. Phys. Discuss.*, 2016, 1–25, doi:10.5194/acp-2016-160, <http://www.atmos-chem-phys-discuss.net/acp-2016-160/>, 2016.
- 765 Li, J., Parchatka, U., Königstedt, R., and Fischer, H.: Real-time measurements of atmospheric CO using a continuous-wave room temperature quantum cascade laser based spectrometer, *Opt. Express*, 20, 7590–7601, doi:10.1364/OE.20.007590, <http://www.opticsexpress.org/abstract.cfm?URI=oe-20-7-7590>, 2012.
- Liakakou, E., Vrekoussis, M., Bonsang, B., Donousis, C., Kanakidou, M., and Mihalopoulos, N.: Isoprene above the Eastern Mediterranean: Seasonal variation and contribution to the oxidation capacity of the atmosphere, *Atmos. Environ.*, 41, 1002–1010, doi:10.1016/j.atmosenv.2006.09.034, <http://www.sciencedirect.com/science/article/pii/S1352231006009721>, 2007.
- 770 Mesarchaki, E., Yassaa, N., D., H., Lutterbeck, H. E., Zindler, C., and Williams, J.: A novel method for the measurement of VOCs in seawater using needle trap devices and GC–MS, *Mar. Chem.*, 149, 1–8, doi:10.1016/j.marchem.2013.12.001, <http://www.sciencedirect.com/science/article/pii/S0304420313002077>, 2014.
- Millet, D. B., Jacob, D. J., Custer, T. G., de Gouw, J. A., Goldstein, A. H., Karl, T., Singh, H. B., Sive, B. C., Talbot, R. W., Warneke, C., and Williams, J.: New constraints on terrestrial and oceanic sources of atmospheric methanol, *Atmos. Chem. Phys.*, 8, 6887–6905, doi:10.5194/acp-8-6887-2008, <http://www.atmos-chem-phys.net/8/6887/2008/>, 2008.
- 780 Müller, M., Mikoviny, T., Jud, W., D’Anna, B., and Wisthaler, A.: A new software tool for the analysis of high resolution PTR-TOF mass spectra, *Chemometrics Intell. Lab. Sys.*, 127, 158–165, doi:10.1016/j.chemolab.2013.06.011, <http://www.sciencedirect.com/science/article/pii/S0169743913001275>, 2013.
- 785 Niki, H., Maker, P. D., Savage, C. M., and Breitenbach, L. P.: An FTIR study of mechanisms for the HO radical initiated oxidation of C<sub>2</sub>H<sub>4</sub> in the presence of NO: detection of glycolaldehyde, *Chem. Phys. Lett.*, 80, 1981.
- Palmer, P. I. and Shaw, S. L.: Quantifying global marine isoprene fluxes using MODIS chlorophyll observations, *Geophys. Res. Lett.*, 32, doi:10.1029/2005GL022592, <http://dx.doi.org/10.1029/2005GL022592>, 2005.
- Paulot, F., Wunch, D., Crouse, J. D., Toon, G. C., Millet, D. B., DeCarlo, P. F., Vigouroux, C., Deutscher, N. M., González Abad, G., Notholt, J., Warneke, T., Hannigan, J. W., Warneke, C., de Gouw, J. A., Dunlea, E. J., De Mazière, M., Griffith, D. W. T., Bernath, P., Jimenez, J. L., and Wennberg, P. O.: Importance of secondary sources in the atmospheric budgets of formic and acetic acids, *Atmos. Chem. Phys.*, 11, 1989–2013, doi:10.5194/acp-11-1989-2011, [www.atmos-chem-phys.net/11/1989/2011/](http://www.atmos-chem-phys.net/11/1989/2011/), 2011.
- 790 Paulson, S. E. and Seinfeld, J. H.: Development and Evaluation of a Photooxidation Mechanism for Isoprene, *J. Geophys. Res.*, 97, 20, 703–20,715, 1992.
- 795 Phillips, G. J., Pouvesle, N., Thieser, J., Schuster, G., Axinte, R., Fischer, H., Williams, J., Lelieveld, J., and Crowley, J. N.: Peroxyacetyl nitrate (PAN) and peroxyacetic acid (PAA) measurements by iodide chemical ionisation mass spectrometry: first analysis of results in the boreal forest and implications for the measurement of PAN fluxes, *Atmos. Chem. Phys.*, 13, 1129–1139, doi:10.5194/acp-13-1129-2013, <http://www.atmos-chem-phys.net/13/1129/2013/>, 2013.
- 800



- Salisbury, G., Williams, J., Holzinger, R., Gros, V., Mihalopoulos, N., Vrekoussis, M., Sarda-Estève, R., Berresheim, H., von Kuhlmann, R., Lawrence, M., and Lelieveld, J.: Ground-based PTR-MS measurements of reactive organic compounds during the MINOS campaign in Crete, July–August 2001, *Atmos. Chem. Phys.*, 3, 925–940, doi:10.5194/acp-3-925-2003, <http://www.atmos-chem-phys.net/3/925/2003/>, 2003.
- 805 Sander, R.: Compilation of Henry's law constants (version 4.0) for water as solvent, *Atmos. Chem. Phys.*, 15, 4399–4981, doi:10.5194/acp-15-4399-2015, <http://www.atmos-chem-phys.net/15/4399/2015/>, 2015.
- Sander, R., Baumgaertner, A., Gromov, S., Harder, H., Jöckel, P., Kerkweg, A., Kubistin, D., Regelin, E., Riede, H., Sandu, A., Taraborrelli, D., Tost, H., and Xie, Z.-Q.: The atmospheric chemistry box model CAABA/MECCA-3.0, *Geosci. Model Dev.*, 4, 373–380, doi:10.5194/gmd-4-373-2011, <http://www.geosci-model-dev.net/4/373/2011/>, 2011.
- 810 Sanhueza, E. and Andreae, M. O.: Emission of formic and acetic acids from tropical Savanna soils, *Geophys. Res. Lett.*, 18, 1707–1710, doi:10.1029/91GL01565, <http://dx.doi.org/10.1029/91GL01565>, 1991.
- Sinha, V., Williams, J., Meyerhöfer, M., Riebesell, U., Paulino, A. I., and Larsen, A.: Air-sea fluxes of methanol, acetone, acetaldehyde, isoprene and DMS from a Norwegian fjord following a phytoplankton bloom in a mesocosm experiment, *Atmos. Chem. Phys.*, 7, 739–755, doi:10.5194/acp-7-739-2007, <http://www.atmos-chem-phys.net/7/739/2007/>, 2007.
- 815 Spanel, P., Diskin, A., Wang, T., and Smith, D.: A {SIFT} study of the reactions of  $\text{H}_3\text{O}^+$ ,  $\text{NO}^+$ , and  $\text{O}_2^+$  with hydrogen peroxide and peroxyacetic acid, *Int. J. Mass Spectrom.*, 228, 269–283, doi:10.1016/S1387-3806(03)00214-8, <http://www.sciencedirect.com/science/article/pii/S1387380603002148>, 2003.
- 820 Staudt, M., Bertin, N., Hansen, U., Seufert, G., Cicciolij, P., Foster, P., Frenzel, B., and Fugit, J.-L.: Seasonal and diurnal patterns of monoterpene emissions from *Pinus pinea* (L.) under field conditions, *Atmos. Environ.*, 31, 145–156, doi:10.1016/S1352-2310(97)00081-2, <http://www.sciencedirect.com/science/article/pii/S1352231097000812>, 1997.
- Stohl, A., Eckhardt, S., Forster, C., James, P., Spichtinger, N., and Seibert, P.: A replacement for simple back trajectory calculations in the interpretation of atmospheric trace substance measurements, *Atmos. Environ.*, 36, 4635–4648, doi:10.1016/S1352-2310(02)00416-8, <http://www.sciencedirect.com/science/article/pii/S1352231002004168>, 2002.
- 825 Stohl, A., Forster, C., Frank, A., Seibert, P., and Wotawa, G.: Technical note: The Lagrangian particle dispersion model FLEXPART version 6.2, *Atmos. Chem. Phys.*, 5, 2461–2474, doi:10.5194/acp-5-2461-2005, <http://www.atmos-chem-phys.net/5/2461/2005/>, 2005.
- 830 Stohl, A., Berg, T., Burkhardt, J. F., Fjérraa, A. M., Forster, C., Herber, A., Hov, Ø., Lunder, C., McMillan, W. W., Oltmans, S., Shiobara, M., Simpson, D., Solberg, S., Stebel, K., Ström, J., Tørseth, K., Treffeisen, R., Virkkunen, K., and Yttri, K. E.: Arctic smoke — record high air pollution levels in the European Arctic due to agricultural fires in Eastern Europe in spring 2006, *Atmos. Chem. Phys.*, 7, 511–534, doi:10.5194/acp-7-511-2007, <http://www.atmos-chem-phys.net/7/511/2007/>, 2007.
- 835 Taddei, S., Toscano, P., Gioli, B., Matese, A., Miglietta, F., Vaccari, F. P., Zaldei, A., Custer, T., and Williams, J.: Carbon Dioxide and Acetone Air Sea Fluxes over the Southern Atlantic, *Environ. Sci. Technol.*, 43, 5218–5222, doi:10.1021/es8032617, <http://dx.doi.org/10.1021/es8032617>, 2009.



- 840 Tyrllis, E., Tymvios, F. S., Giannakopoulos, C., and Lelieveld, J.: The role of blocking in the summer 2014 collapse of Etesians over the eastern Mediterranean, *J. Geophys. Res. - Atmos.*, 120, 6777–6792, doi:10.1002/2015JD023543, <http://dx.doi.org/10.1002/2015JD023543>, 2015.
- Veres, P. R., Faber, P., Drewnick, F., Lelieveld, J., and Williams, J.: Anthropogenic sources of VOC in a football stadium: Assessing human emissions in the atmosphere, *Atmos. Environ.*, 77, 1052–1059, doi:10.1016/j.atmosenv.2013.05.076, <http://www.sciencedirect.com/science/article/pii/S1352231013004494>, 2013.
- 845 Williams, J., Holzinger, R., Gros, V., Xu, X., Atlas, E., and Wallace, D. W. R.: Measurements of organic species in air and seawater from the tropical Atlantic, *Geophys. Res. Lett.*, 31, doi:10.1029/2004GL020012, <http://dx.doi.org/10.1029/2004GL020012>, 2004.
- Xu, X., Stee, L. L. P., Williams, J., Beens, J., Adahchour, M., Vreuls, R. J. J., Brinkman, U. A., and 850 Lelieveld, J.: Comprehensive two-dimensional gas chromatography (GC × GC) measurements of volatile organic compounds in the atmosphere, *Atmos. Chem. Phys.*, 3, 665–682, doi:10.5194/acp-3-665-2003, <http://www.atmos-chem-phys.net/3/665/2003/>, 2003.
- Yañez Serrano, A. M., Nölscher, A. C., Williams, J., Wolff, S., Alves, E., Martins, G. A., Bourtsoukidis, E., Brito, J., Jardine, K., Artaxo, P., and Kesselmeier, J.: Diel and seasonal changes of Biogenic Volatile Organic 855 Compounds within and above an Amazonian rainforest site, *Atmos. Chem. Phys. Discuss.*, 14, 29 159–29 208, doi:10.5194/acpd-14-29159-2014, <http://www.atmos-chem-phys-discuss.net/14/29159/2014/>, 2014.
- Yang, M., Nightingale, P. D., Beale, R., Liss, P. S., Blomquist, B., and Fairall, C.: Atmospheric deposition of methanol over the Atlantic Ocean, *Proc. Natl. Acad. Sci. USA*, 110, 20 034–20 039, doi:10.1073/pnas.1317840110, <http://www.pnas.org/content/110/50/20034.abstract>, 2013.
- 860 Yang, M., Beale, R., Liss, P., Johnson, M., Blomquist, B., and Nightingale, P.: Air–sea fluxes of oxygenated volatile organic compounds across the Atlantic Ocean, *Atmos. Chem. Phys.*, 14, 7499–7517, doi:10.5194/acp-14-7499-2014, <http://www.atmos-chem-phys.net/14/7499/2014/>, 2014.



**Table 1.** Averaged data of VOCs, O<sub>3</sub> and CO and their standard deviation in pptv for periods reached by air from eastern or western regions. For the calculation only data above the detection limit ( $3\sigma$ ) were used and n represents the number of points above this limit.

Compound	Eastern air mass	Standard deviation (east)	Western air mass	Standard deviation (west)
Methanol	3545 (n = 1687)	949	2571 (n = 908)	694
Acetonitrile	112 (n = 1695)	23	108 (n = 908)	29
Acetaldehyde	370 (n = 1625)	146	246 (n = 907)	92
Acetone	2659 (n = 1695)	576	1994 (n = 908)	342
Acetic acid	1280 (n = 1566)	598	778 (n = 851)	312
Dimethylsulfide	103 (n = 1695)	40	117 (n = 882)	60
Isoprene	101 (n = 941)	62	78 (n = 498)	55
Methylvinylketone	43 (n = 910)	31	41 (n = 348)	40
Methylethylketone	127 (n = 1695)	32	81 (n = 908)	21
Benzene	37 (n = 1515)	16	24 (n = 230)	11
Toluene	19 (n = 462)	21	17 (n = 72)	7
Total xylenes	26 (n = 427)	33	49 (n = 99)	124
Total trimethylbenzenes	19 (n = 223)	29	27 (n = 96)	74
Total monoterpenes	65 (n = 1326)	56	49 (n = 736)	42
Ozone	73588 (n = 2036)	9441	61844 (n = 994)	8627
CO	107274 (n = 2054)	9868	91361 (n = 1003)	6902



**Table 2.** Slope, intercept and correlation coefficient ( $r^2$ ) of different compounds separated in air masses from Eastern and Western Europe

Eastern air masses	Western air masses
Methanol vs. acetone <i>slope</i> = 1.8, <i>intercept</i> = -1.1, $r^2$ = 0.76	Methanol vs. acetone <i>slope</i> = 2.8, <i>intercept</i> = -3.0, $r^2$ = 0.62
Acetic acid vs. methanol <i>slope</i> = 0.54, <i>intercept</i> = -0.64, $r^2$ = 0.53	Acetic acid vs. methanol <i>slope</i> = 0.37, <i>intercept</i> = -0.18, $r^2$ = 0.57
Acetic acid vs. acetone <i>slope</i> = 1.0, <i>intercept</i> = -1.5, $r^2$ = 0.81	Acetic acid vs. acetone <i>slope</i> = 1.1, <i>intercept</i> = -1.4, $r^2$ = 0.52
Methanol vs. ozone <i>slope</i> = 0.056, <i>intercept</i> = -0.60, $r^2$ = 0.32	Methanol vs. ozone <i>slope</i> = 0.022, <i>intercept</i> = 1.2, $r^2$ = 0.08
Methanol vs. CO <i>slope</i> = 0.065, <i>intercept</i> = -3.4, $r^2$ = 0.45	Methanol vs. CO <i>slope</i> = 0.067, <i>intercept</i> = -3.6, $r^2$ = 0.44
Acetone vs. ozone <i>slope</i> = 0.036, <i>intercept</i> = 0.017, $r^2$ = 0.36	Acetone vs. ozone <i>slope</i> = 0.0067, <i>intercept</i> = 1.6, $r^2$ = 0.04
Acetone vs. CO <i>slope</i> = 0.046, <i>intercept</i> = -2.3, $r^2$ = 0.61	Acetone vs. CO <i>slope</i> = 0.030, <i>intercept</i> = -0.80, $r^2$ = 0.52
Acetic acid vs. ozone <i>slope</i> = 0.032, <i>intercept</i> = -1.1, $r^2$ = 0.26	Acetic acid vs. ozone <i>slope</i> = 0.018, <i>intercept</i> = -0.35, $r^2$ = 0.25
Acetic acid vs. CO <i>slope</i> = 0.041, <i>intercept</i> = -3.1, $r^2$ = 0.46	Acetic acid vs. CO <i>slope</i> = 0.024, <i>intercept</i> = -1.4, $r^2$ = 0.28
Ozone vs. CO <i>slope</i> = 0.92, <i>intercept</i> = -25, $r^2$ = 0.30	Ozone vs. CO <i>slope</i> = 1.9, <i>intercept</i> = -110, $r^2$ = 0.14

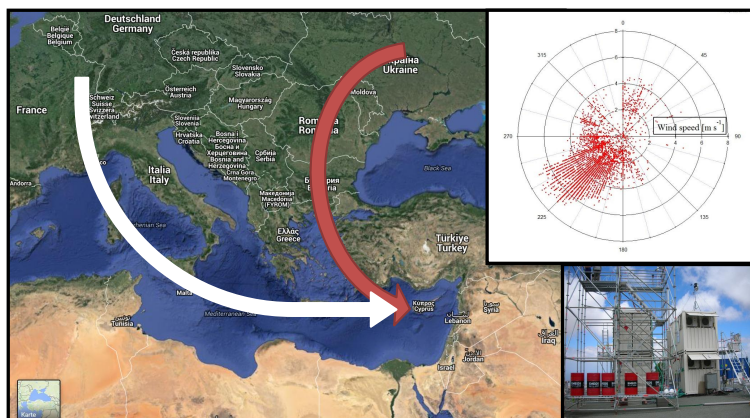


**Figure 1.** Map of the Mediterranean basin (Source: Google). The white arrow shows the inflow from Western and the red the inflow from Eastern Europe. On the right hand side a wind rose displaying the dominant wind direction and a picture of the laboratory containers can be seen.

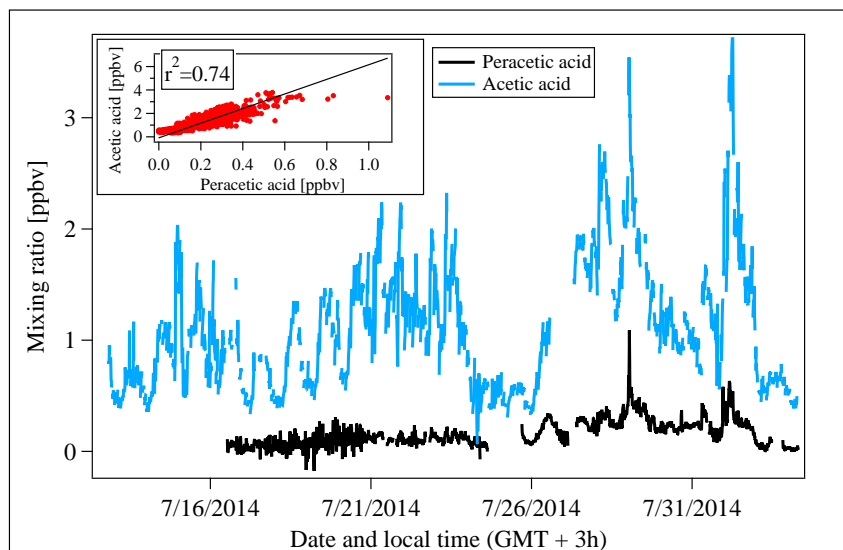


**Figure 2.** Time traces of peracetic acid measured by CIMS and acetic acid measured by PTR-TOF-MS (10 min mean values). The upper left plot shows the correlation between both compounds from 26 July until the end of the campaign.

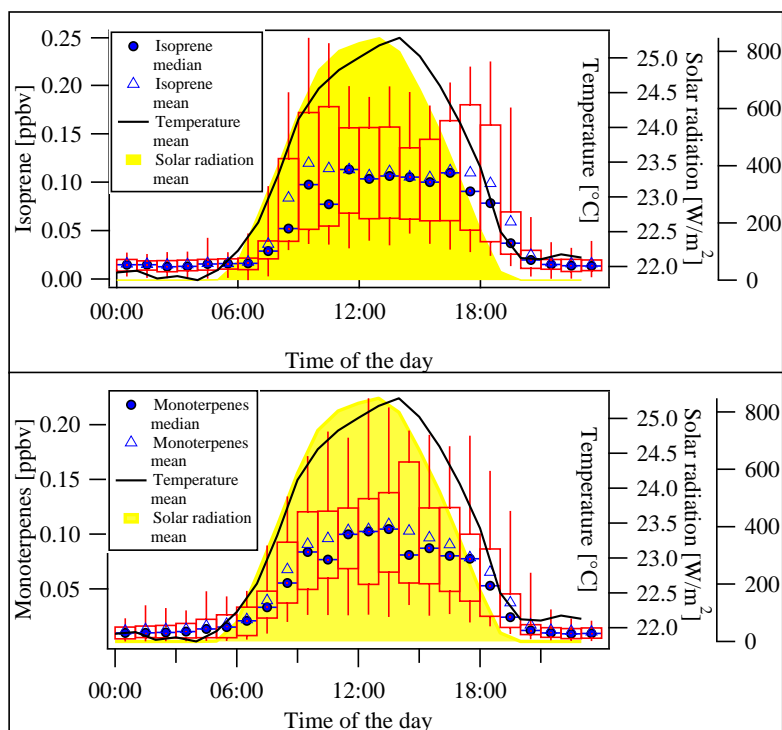


**Figure 3.** Box and whiskers plots of isoprene and the sum of monoterpenes. The box contains 50 % of the data. 25 % of the data lie below the lower end of the box, 75 % below the upper end. The whiskers present the 5–95 % range of the data.

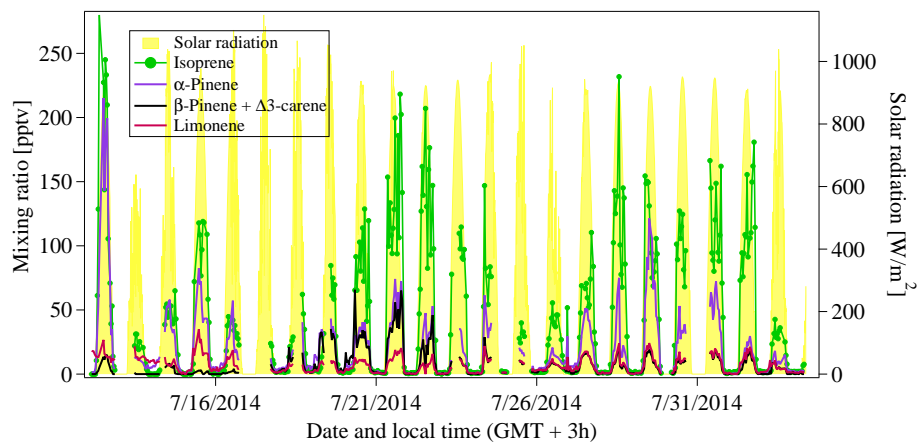


**Figure 4.** Time traces of isoprene and different monoterpenes in pptv measured by GC-MS as well as solar radiation in  $\text{Wm}^{-2}$

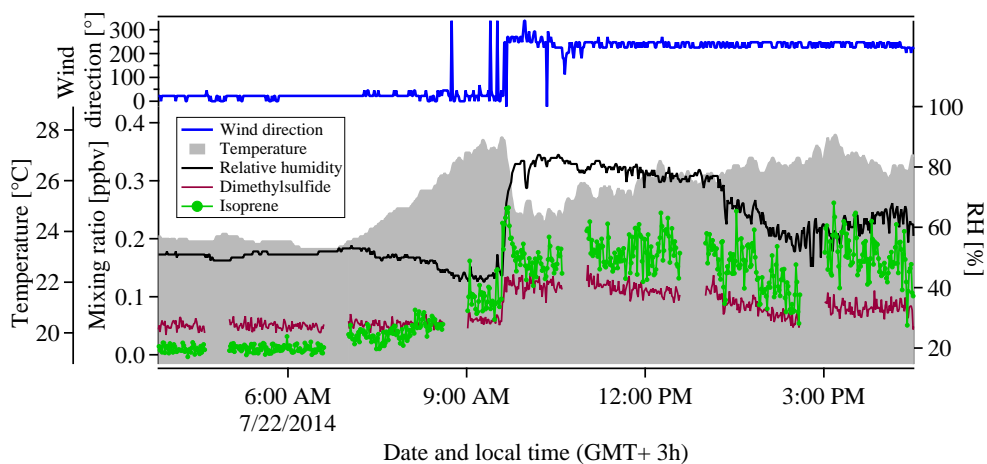


**Figure 5.** Mixing ratios of isoprene and DMS in ppbv as well as wind direction in  $^{\circ}$ , temperature in  $^{\circ}$ C and relative humidity in % as a function of time with an one minute time resolution

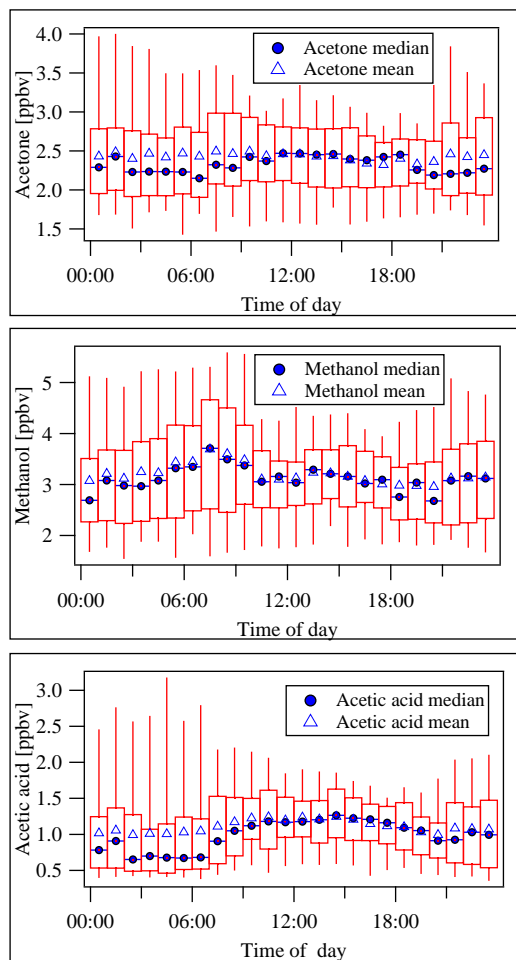


**Figure 6.** Box and whiskers plot of acetone, methanol and acetic acid. The box contains 50 % of the data. 25 % of the data lie below the lower end of the box, 75 % below the upper end. The whiskers present the 5–95 % range of the data.

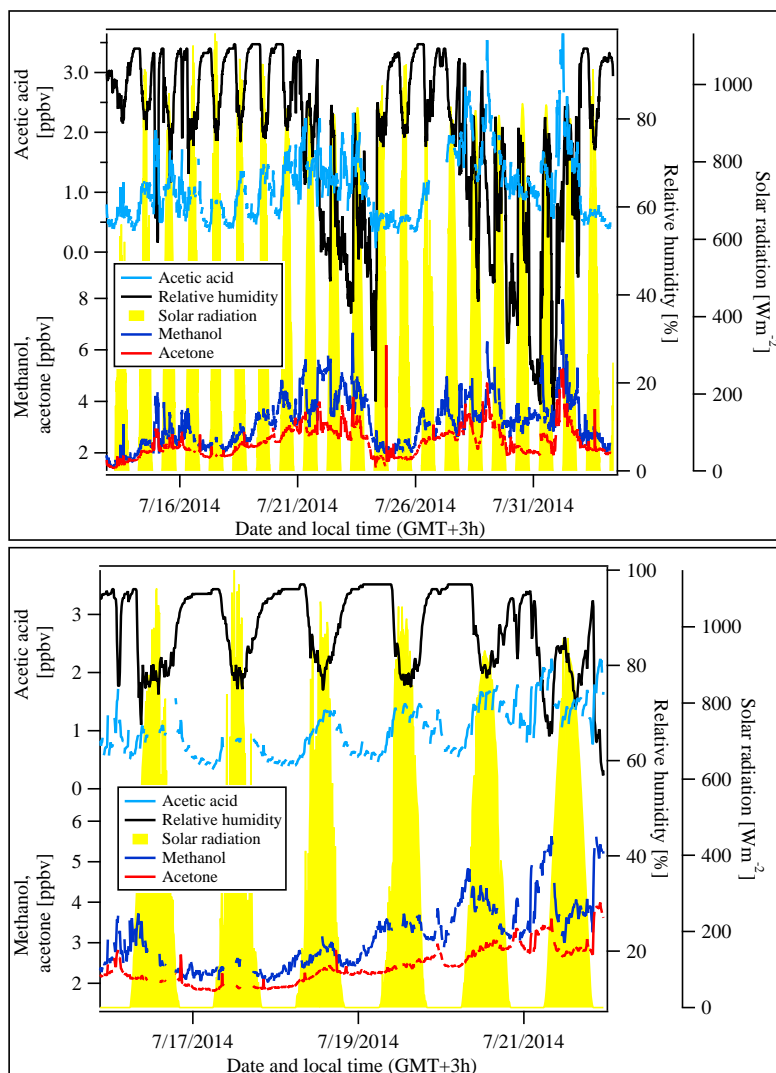


**Figure 7.** Mixing ratios of acetic acid, acetone and methanol in ppbv (10 min mean values), relative humidity in % and solar radiation in  $Wm^{-2}$  as a function of time. The lower panel shows a detail from 16 to 21 July.

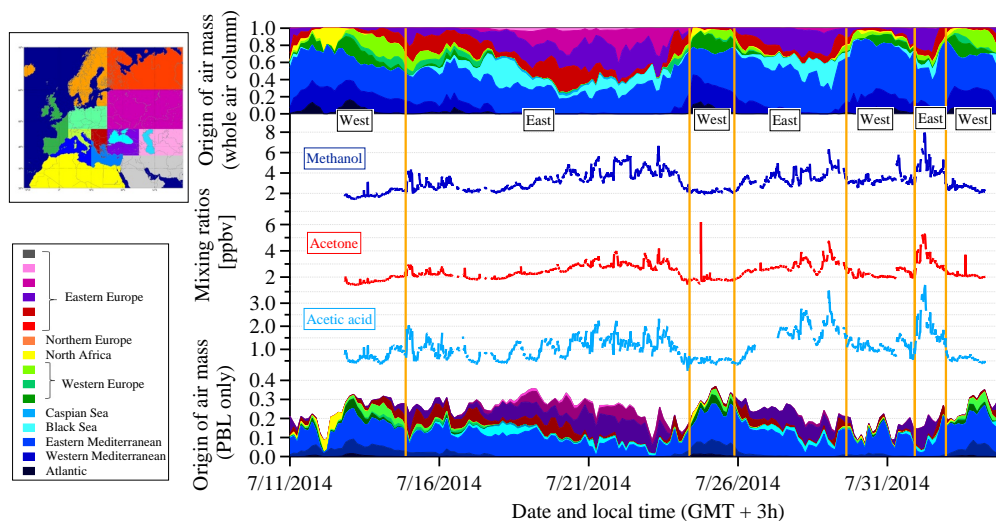


**Figure 8.** Allocation of Europe into specific regions (upper left panel) as well as traces of methanol, acetone and acetic acid in ppbv (10 min mean values) and modeled data of the area of influence, given in fractions of 1. The upper part of the right panel refers to the whole air column, while the lower part of the right panel represents the PBL, only.

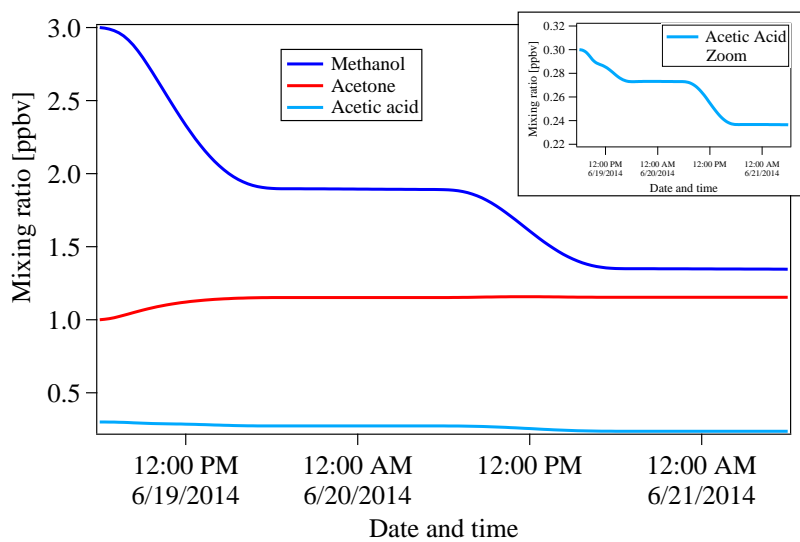


**Figure 9.** Modeled mixing ratios of acetic acid, acetone and methanol in ppbv over the period of 48 h starting at 6 am. Initial values originate from the MOM chemistry in the global model EMAC (Jöckel et al., 2016).

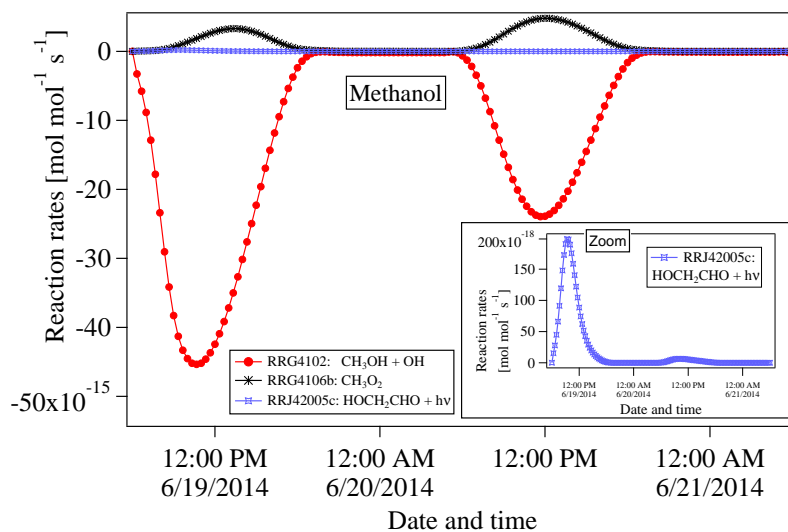


**Figure 10.** Rates for reactions influencing the mixing ratio of methanol. Further explanation of the reactions can be found in the supplement.

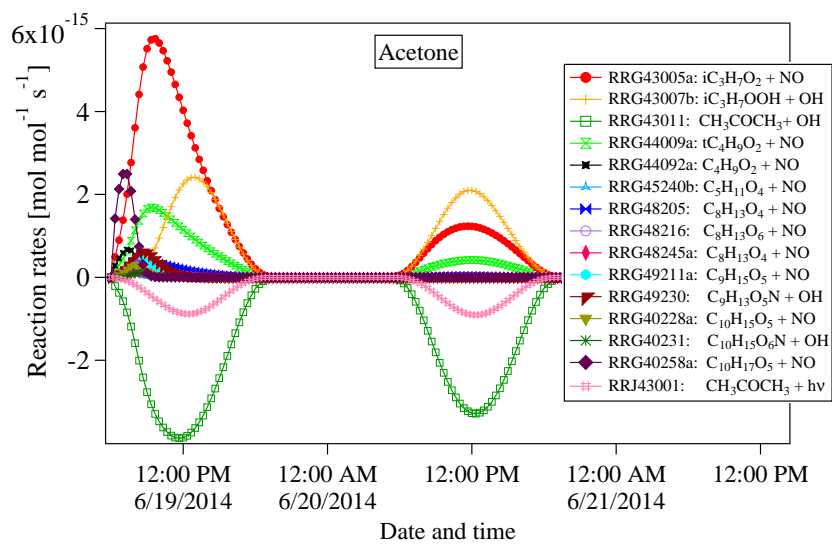


**Figure 11.** Rates for reactions influencing the mixing ratio of acetone. Further explanation of the reactions can be found in the supplement.

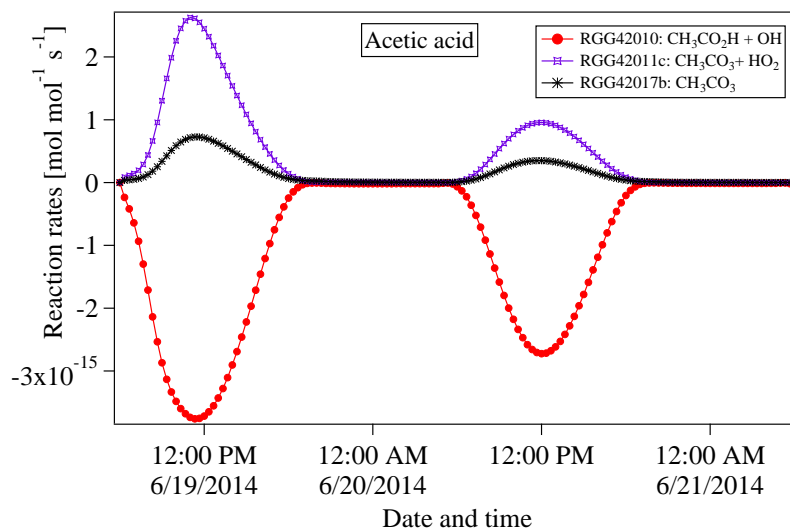


**Figure 12.** Rates for reactions influencing the mixing ratio of acetic acid. Further explanation of the reactions can be found in the supplement.

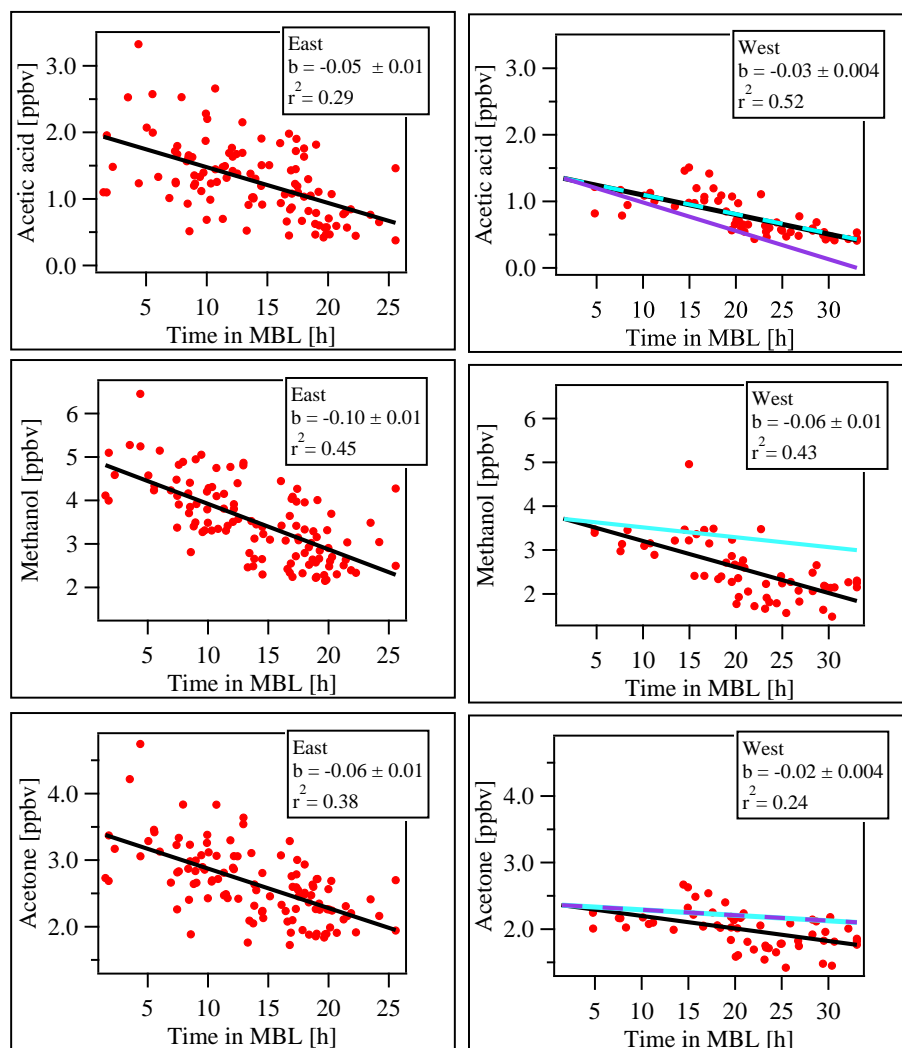


**Figure 13.** Data of acetone, methanol and acetic acid separated by eastern and western air masses, plotted against the time in the MBL. The data were fitted using a linear fit algorithm (black line). The light blue lines refer to calculated loss rates using dry deposition rates from the EMAC model. The violet lines represent loss rates adjusted by solubility relative to methanol.

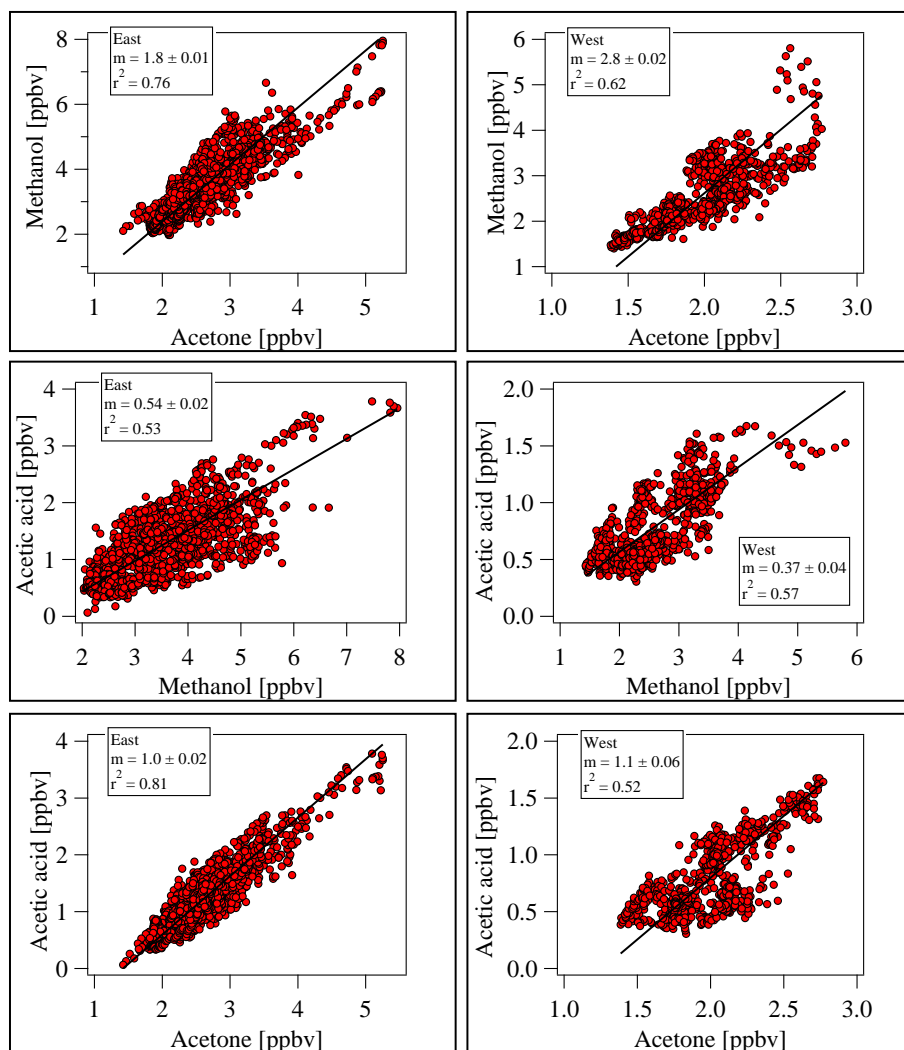


**Figure 14.** Correlations between the OVOCs separated by eastern and western flow regimes. A bivariate fitting method was applied.

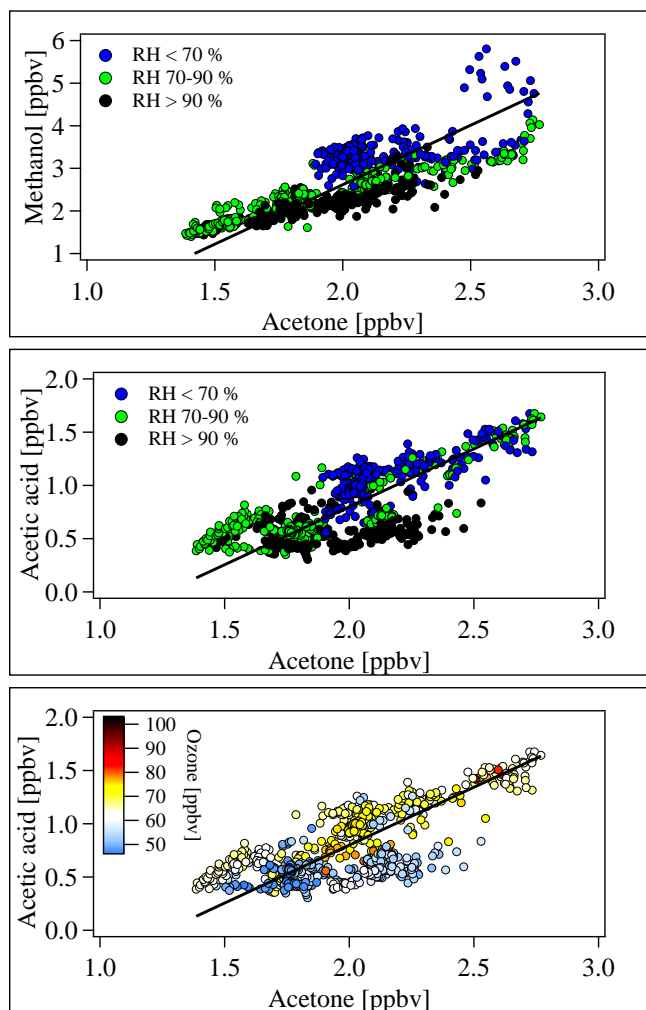


**Figure 15.** Correlation plots exclusively from western air masses were color coded by ozone data and relative humidity to show different branches

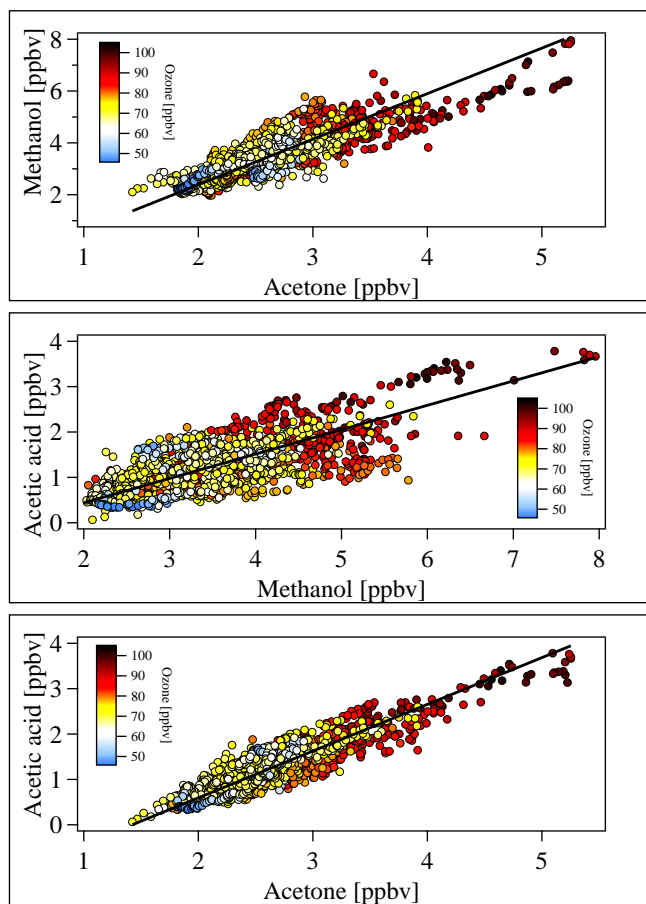


**Figure 16.** Correlations plots solely from eastern flow regimes were color coded by ozone data